

D34

N79-15622

**ROLL TRACKING EFFECTS OF G-VECTOR TILT AND VARIOUS
TYPES OF MOTION WASHOUT**

Henry R. Jex and Raymond E. Magdaleno
Systems Technology, Inc.
Hawthorne, California

and

Andrew M. Junker
6570th Aerospace Medical Research Lab, EM Branch
Wright-Patterson AFB, Ohio

SUMMARY

The aim of this research was to discover the basic effects on pilot roll tracking behavior, performance, and impressions for several types of motion-reducing logic ("washouts") used in moving-base simulators. It was a joint program between the 6750 Aerospace Medical Research Laboratory (AMRL-EM Branch) and Systems Technology, Inc.

The experiments were performed on the AMRL Dynamic Environment Simulator (DES), in the roll degree of freedom only. The g-vector was oriented both normally (pilot erect, tilt cue present) and 90 deg nose-up (pilot supine, no tilt cue). Washout filters included: second order, first order, attenuated first order, attenuated, and static (fixed base).

In a dogfight scenario, the task was to follow the target's roll angle while suppressing gust disturbances. The two independent inputs (interleaved sum-of-sines) enabled identification of both the visual and motion response parameters of the pilot by the STI Model Fitting Program (MFP'77). A 12-parameter multiloop model structure fitted includes separate visual and roll motion sensing channels, with a common neuromuscular actuator block.

Excellent describing function and performance data as well as subjective impressions were obtained on four non-pilot subjects, each well trained in the "real-world" case (full motion; 90 deg nose-up). All subjects adopted the same behavioral strategies in following the target while suppressing the gusts, and the MFP-fitted math model response was generally within one "data symbol width."

The results include the following:

- Comparisons of full roll motion (both with and without the spurious gravity tilt cue) with the static case. These motion cues help suppress disturbances with little net effect on the visual performance. Tilt cues were clearly used by the pilots but gave only small improvement in tracking errors.

- The optimum washout (in terms of performance close to "real world," similar behavioral parameters, significant motion attenuation (60 percent), and acceptable motion "fidelity") was the combined attenuation and first-order washout.
- Various trends in parameters across the motion conditions were apparent, and are discussed with respect to a comprehensive model for predicting pilot adaptation to various roll motion cues.

The detailed data base (spectra, remnant, describing functions, model fits) are compiled in a separate document available to interested researchers through AMRL-EM.

INTRODUCTION

Objectives and Background

A joint experimental/analytical effort by the Aerospace Medical Research Laboratory (AMRL/EM) and Systems Technology, Inc. (STI) was conducted to define a pilot's use of motion cues in moving-base simulators free to rotate only in the roll degree of freedom. This situation provides the pilot an intrinsically spurious roll attitude or "tilt" cue. This effect can be reduced by "washing out" the cab motion so the cab always tends to return to an upright orientation, although this distorts the true angular motions. The optimization of the washout dynamics to achieve the best compromise between realistic roll rate cues and suppression of the spurious tilt cue is an important facet of the immediate future work to be done in the AMRL/EM laboratory.

The basic objective was to determine what form and degree of washout dynamics achieves the highest simulation realism, while engendering true-to-life behavior of the pilot, and producing the correct performance effects due to environmental stressors. Longer range objectives include the possible correlation of these experiments with other ground-based simulations and later with in-flight experiments.

To accomplish the above objectives this investigation had to consider two basic problems in moving-base simulation: the use of motion cues by the pilot in the actual ("real world") case and the effects of spurious motion cues in modifying that usage in the simulator. A brief examination of the piloting task involved in the first problem is useful before proceeding to the second.

Consider a situation of primary interest to the Air Force — air-to-air combat — and focus upon the pilot's response to the dynamic (non-steady) components of motion. Assume that, initially, the pilot has his wings lined up with those of a target aircraft that he perceives against a murky or night-time background (no horizon visible). In this "impoverished display" situation he can visually perceive only the difference (error) between the target's wings and his own. Further, the pilot has two tasks to perform, often simultaneously:

- a. Regulate (suppress) disturbances, e.g., due to gusts or swirls from the target's wingtip vortices. In this task the pilot's role is to reduce motions, and if he suppresses the gusts with small error, the physical motions become small.
- b. Track (follow) the target roll motions (e.g., by keeping one's wings parallel with the target). In this task the pilot's role is to produce motions, and if he tracks with small error, the physical motions become larger (approaching the target motions).

In the general case, where both inputs are present, the pilot is faced with a continual conflict between reducing disturbance motion and producing correct following motions. The figure-of-merit (at least in air combat and landing tasks) is primarily low roll error (and, perhaps, limited roll acceleration or its rough equivalent — aileron control deflection). Because multiple sensory feedbacks are involved, with more than one input, the problem is a multiloop one, and this greatly complicates the control system analysis as well as the attempt to infer the pilot's behavioral "structure" and parameters, as will be demonstrated, herein.

Most of the earlier research in measuring the use of visual and motion cues, such as that of Stapleford, et al (Ref. 1) and Shirley (Ref. 2), tended to have either the target input or disturbance, as dominant, such that the possible cue conflicts were minimized. Stapleford, et al were able to infer the separate visual and motion pathway dynamics by using mathematically independent target and disturbance inputs comprising sums-of-sinusoids interleaved in frequency, then interpolating between frequencies to solve the simultaneous vector equations required to untangle the loops (this process will be shown later herein). However, these pioneering results were not fitted in any form suitable for efficient use. Thus, the secondary objectives of this program were to improve the reduction and analysis of multi-sensory manual control data, and to structure and parameterize the results. Here, where the target following and disturbance motions were comparable, in bandwidth and amplitude, new techniques were required.

Such a situation seem natural for an optimal control model of the human operator, and Levison, working with AMRL experimenters has put forth a first-cut at just such a model in Refs. 3 and 4. The forcing functions were either target inputs or disturbances, and effects similar to Stapleford's and Shirley's were obtained. Whether or not their (implicitly) assumed feedback structure is valid is hard to say without more data on the all important dual-input case treated here.

In another approach Zacharias (Ref. 5) has tackled the problem of sensory conflict of visual and vestibular sensors in conjunction with regulation of purely visual, purely motion or conflicting cue situations, and has speculated on a cue-conflict resolving model for the human operator, in the yaw-only degree of freedom. Testing the validity of such cue-conflict-resolution approaches as these requires a very solid data base to exercise one's model against, and this is still largely lacking. In light of the above needs, a

third objective was to establish a very solid and comprehensive data base, using inputs, controlled elements, and washouts that were analytically tractable and fairly linear, so that future validation of cue-utilization models would be facilitated.

Scope

To meet these objectives, the AMRL Dynamic Environmental Simulator (DES) was employed, which permits pilot rolling motions with his rolling axis horizontal (normal spurious tilt cues present) as well as vertical (tilt cues absent). Details are given later. The scenario selected was that of air-combat with a set of fairly sluggish aircraft roll dynamics, so that motion cues would be useful. As will be described, the target and disturbances were carefully designed to provide strong motion-usage conflicts as well as easy analytical modeling. Several motion cases, ranging from full motion, various washouts to fixed base were included. Based on prior work, a plausible structure for the pilot's use of visual and motion inputs was proposed, and a newly developed technique was used to fit these model parameters quite precisely to the frequency-domain data.

We show how some of the past results are explained on the basis of differences in the apparent "opened-loop" transfer functions for target vs. disturbance inputs, despite identical pilot behavior with respect to either by itself.

To obtain reliable measurements, worth fitting by the relatively high-order models selected, extremely consistent pilot behavior is necessary. This was obtained by a combination of the sluggish controlled element (which had a fairly well-defined optimum strategy) and very well-trained subjects.

The results show clear answers to the questions raised earlier, when analyzed with respect to various performance and behavioral (dynamic) parameters, and some interesting trends are evident in the pilot parameters vs. motion measures, even for fairly small motions. Nevertheless, this report does not attempt to interpret these covariations in terms of an overall model of operator adaptation to pure and distorted motion feedbacks.

EXPERIMENTAL DESIGN

Approach

As noted in the introduction, there were two facets of roll motion-cue usage to be investigated: "real-world" motion vs. no-motion and distortions of real-world motion by various washout filters. In the actual flight case, where gradual bank angles result in translation of the aircraft, there is no way to tell vertical by seat-of-the-pants or other vestibular sensors. A set of realistic rolling cues were provided by tipping the roll-axes of the simulator 90 deg nose upward so that the spurious tilt cues were absent. This full-motion at 90 deg inclined roll axis (F-90) case was given the most

practice and became the "real-world" reference for all other motion cases. By comparing it with the static case, the basic effects of motion were revealed. To check effects of the conflicts between target following vs. disturbance regulation, both forcing functions were given alone and together (dual input) for the F90 case. If the dual case gave similar data as either input alone, then the dual input could be used throughout, with consequent savings in runs and data analysis.

The washouts in roll-only simulators are used for two main purposes, a) to reduce the tilt cues (largely a low frequency effect) and b) to reduce any or all motions (accelerations, rates, displacements) to fit into a limited capability simulator, always with a horizontal orientation of the roll-axis. Consequently the effects of simulated roll only motions were covered by the full motion at 0 deg roll axis inclination and various washouts — all selected to give substantial reduction in roll displacement.

To keep the number of runs within bounds, it was decided to keep constant the plant and the spectrums of forcing functions; and to try only one variation of each washout filter scheme.

Control Task

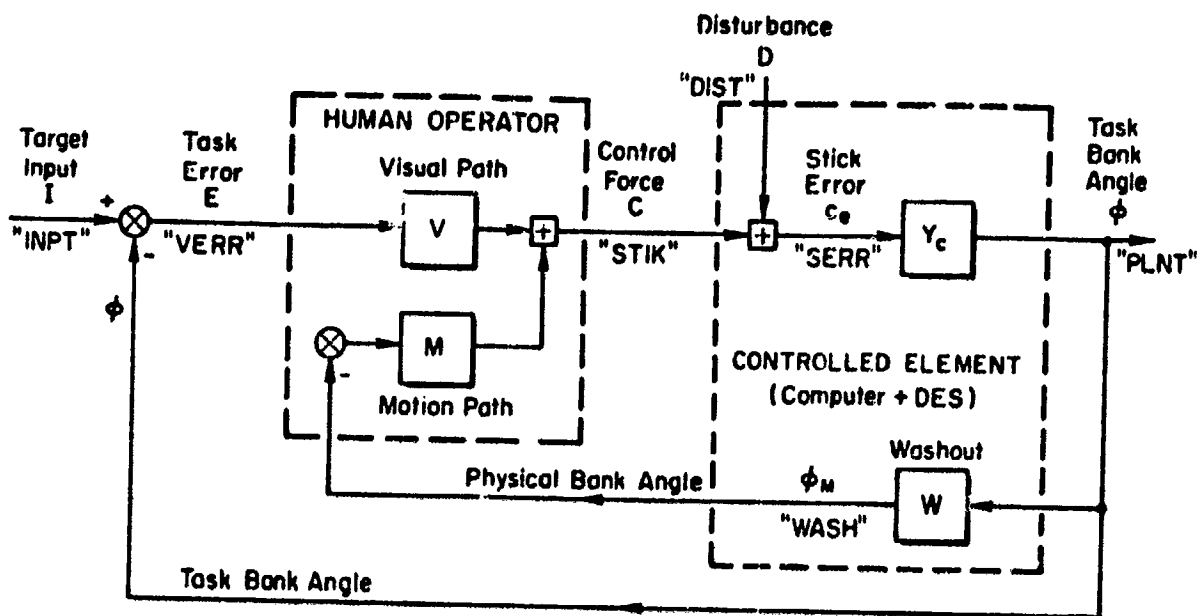
Block Diagram — a scenario with high face validity relevant to Air Force problems is air-to-air gunnery. In a modern high thrust/weight fighter, combat maneuvers take place at all flight path angles, hence the horizon is relatively unimportant. The main criterion for accurate tail chase is to match the roll angle of the target aircraft. The pilot is attempting to follow an evasive target while at the same time he may be buffeted by gusts, a component of which could be wing tip vortices of the target. To simplify the simulation and subsequent modeling and interpretation, a compensatory display (error only) was used and the subjects were instructed to minimize the bank angle error.

Fig. 1-a illustrates the basic elements involved: the Human Operator, Controlled Element, and Washout dynamics. The multiloop nature is evident in that the Motion Path senses physical (inertial) bank angle while the Visual Path senses the error between target and task bank angle. (The four-character "names" on the signals in Fig. 1 represent the Fourier coefficients and are used to label some power spectra and describing functions later in this report).

Controlled Element

The controlled element (Eq. 1 on Fig 1-b) represents an approximation to the roll dynamics of a fighter. The Roll Subsidence mode, having a time constant of $1/1.6 = 0.63$ sec, is typical of a loaded fighter (i.e., with external stores). This value was selected as it would require a significant amount of lead generation by the pilot, because the Crossover-Law for human operator equalization (e.g., Ref. 5) predicts that in such cases the ideal pilot lead

a. Block Diagram Showing Definitions of Elements and Signals



b. Controlled Element Transfer Function

$$Y_c(s) \equiv \frac{\phi}{c_e} \doteq 17 \frac{\overbrace{(-s/25 + 1)}^{\text{DES Lags}}}{s \underbrace{\left(\frac{s}{1.6} + 1\right)}_{\text{Spiral Mode}} \underbrace{\left(\frac{s}{5} + 1\right)}_{\text{Roll Subsidence}} \underbrace{\left(\frac{s^2 + 2(.3)s + 1}{11^2 + 11}\right)}_{\text{"Servo" Lag "Structural" Mode}}} \quad \left(\frac{\text{deg/sec}}{16}\right) \quad (1)$$

ORIGINAL PAGE IS
OF POOR QUALITY

Figure 1. Roll Tracking Task Block Diagram and Transfer Function

C-6

would be about $T_L \doteq T_R \doteq 0.5-0.7$ sec. The "Structural Mode" and "DES lags" represent the unavoidable and measured response characteristics of the DES motion simulator, while the "Servo" Lag represents actuation lags of a (poor) aircraft control system. It was raised to 0.2 sec to prevent excessive acceleration or rate commands to the DES which would cause its drives to operate in a partly saturated (hence nonlinear) manner.

Analysis of this controlled element showed that it requires a fairly tightly constrained pilot equalization, with some lead to offset the roll-subsidence lag, but not too much or else the structural mode and lag elements would destabilize the system. Thus, there was a clearly optimum control strategy for the subjects to learn, which was important because they were not experienced pilots.

Forcing Functions

Quasi-random target and disturbance inputs were constructed from eight sinusoids each (Table 1). The frequencies were selected so as to have an integer number of cycles in the run length as shown. To assure statistically independent inputs, target and disturbance frequencies were interleaved, yet each was approximately evenly spaced on a log-frequency plot. After these choices were made the amplitudes were "shaped" to simulate a random noise process that would result from white noise being filtered by the shaping filter forms given in Table 1. Finally, these "shaped amplitudes" were scaled so as to give the listed rms and peak amplitude values.

The target's shaping filter was selected to simulate a low pass spectrum typical of an evasive target. The disturbance's shaping filter was selected so that under static conditions (and, as further shaped by the controlled-element) the spectral content and rms values would be nearly equal to that of the target, as seen on the error display. Thus the pilot could not use input frequency properties to separate target motions from disturbance motions.

Multiloop Pilot Model and Identification Procedure

Analysis. — The measurement problems involved in the multiloop system of Fig. 1-a can be illustrated by examining the task error components resulting from target and disturbance inputs, shown in Fig. 2.

First consider the static case, where the Motion Path is inoperative: $M(j\omega) = 0$. Then the task error vector (frequency response function) becomes that given by Eq. 2 in Fig. 2 (for convenience, we have dropped the arguments $s = j\omega$ in each of the inputs and transfer functions; $E(j\omega) = E$, etc.).

Equation 2 has been written in the form of a conventional single loop system, wherein the [] term is the closed-loop error-to-input describing function, so the product $V \cdot Y_c$ is recognized as the open-loop describing

TABLE 1. FORCING FUNCTIONS FOR DUAL INPUT RUNS

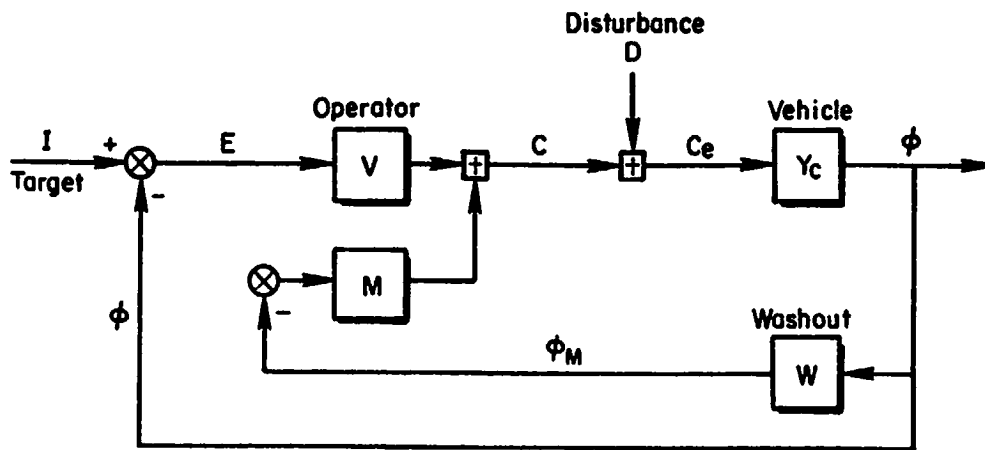
TARGET (rms = 7.1 deg)*			DISTURBANCE (rms = .74 lb = 3.4 N)*		
$\frac{\text{Cycles}}{\text{Run Length}\dagger}$	ω (rad/sec)	A_{dB} 0 = 1. deg	$\frac{\text{Cycles}}{\text{Run Length}}$	ω (rad/sec)	A_{dB} 0 = 1. lb
5	0.19	13.6	9	0.35	-20.6
13	0.50	11.6	17	0.65	-16.5
23	0.88	8.7	30	1.15	-13.6
37	1.42	5.6	49	1.88	-11.4
63	2.42	1.0	83	3.18	-9.7
107	4.10	-5.8	141	5.41	-9.2
182	6.98	-14.4	241	9.24	-10.0
309	11.85	-24.4	410	15.72	-11.7
SHAPING FILTER FORM					
$\frac{1}{(s+0.5)(s+1.7)(s+5.0)}$			$\frac{s}{(s+0.5)(s+5.)}$		

* For single input runs the values were increased by $\sqrt{2}:1$
 † Run length = 163.84 sec

function, G_{OL} for purely visual feedbacks. Recall that increasing the magnitude of G_{OL} reduces tracking errors, etc.

Similarly, in hypothetical situations where the operator would close his eyes and operate solely on motion cues ($V = 0$), the task errors would be given by Eq. 3 in Fig. 2. The input is unaffected, while the disturbances are suppressed.

When both visual and motion paths are active the multiloop relationships become more complex, but can still be written so as to reveal the effective opened-loop dynamics (similar to Eqs. 2 and 3), as shown in Eq. 4. Now, however, the "opened-loop" describing function for target errors (G_T , of Eq. 4a) contains the closed-motion loop $1/(1 + MWY_C)$, while G_D for the disturbance errors contain the sum of motion and visual effects $(V + MW)Y_C$.



Note: All blocks and signals are vector functions of frequency:
 $E = E(j\omega)$ etc.

For Visual only: (Static; $M \equiv 0$)

$$E = (I - DY_c) \left[\frac{(E/I)_{CL}}{1 + VY_c} \right] \quad (2)$$

Open-loop DF: " G_{OL} " for Visual Loop alone

For Motion Only: (Eyes closed; $V \equiv 0$)

$$E = I - DY_c \left[\frac{1}{1 + MWY_c} \right] \quad (3)$$

Open-loop DF: G_{OL} for Motion Loop alone

For Visual-Plus-Motion:

$$E = I \left[\frac{1}{1 + G_I} \right] + (-DY_c) \left[\frac{1}{1 + G_D} \right] \quad (4a)$$

where "Opened-loop" DF's

$$G_I = \frac{VY_c}{1 + MWY_c} \quad (4b)$$

$$G_D = (V + MW)Y_c \quad (4c)$$

Figure 2. Closed-loop Error Relationships to Target and Disturbance Inputs for Various Single and Multiloop Structures

In the single loop cases of Eqs. 2 and 3 a high-gain (V or M) reduces errors, but in the multiloop case there is a conflict:

- A high-gain motion feedback (large M) reduces the disturbance errors via Eqs. 4a and 4c, but increases the target errors via 4a and 4b.
- A high-gain visual loop (large V) reduces both error components.
- The optimum strategy (to minimize E) is a complicated function of the spectra of I and $D \cdot Y_c$, as well as of Y_c and W .

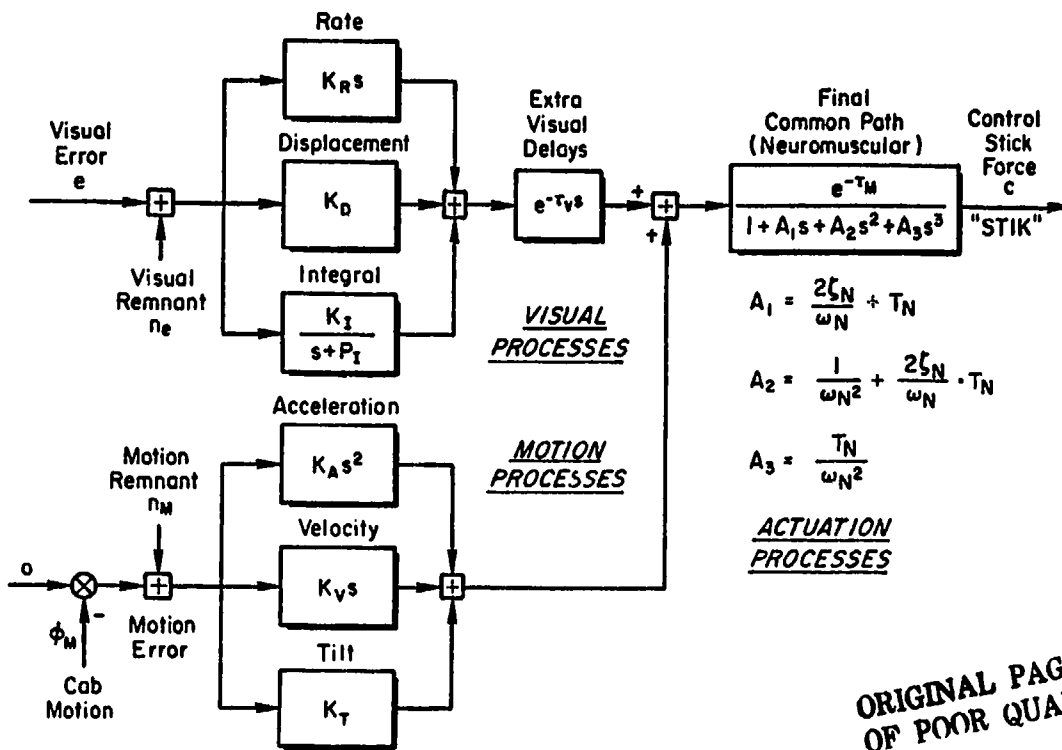
These are the analytical expressions for the qualitative motion/visual cue conflict mentioned in the introduction. Further, notice that analytically opening the loop for either target or disturbance inputs will give different apparent "opened-loop" describing functions (Eqs. 4b vs. 4c) even with identical V and M operations in both equations. This has led in the past to some misinterpretation of results for mostly-target or mostly disturbance inputs.

Finally, it can be seen that, knowing the vehicle and washout dynamics (Y_c and W) and with simultaneous independent inputs I and D , the independent estimates of the visual and motion operations (V and M) are theoretically possible if the signals are not confounded with noise. The temptation to measure V and M from static and motion-only runs, respectively, is precluded by the adaptive nature of the human operator. In general, the pilot will adopt different parameter values for his gains, leads and lags in the above special cases compared to the combined case, as will be shown later.

Model Structure and Parameters. — The criteria for selecting the model structure were that it be:

1. The simplest form capable of capturing all of the significant frequency-domain characteristics of the measured data, both with and without motion.
2. Have components structurally related to previously well known visual-motor elements, such as neuromuscular (NM) and, central-nervous system (CNS) components, as well as motion sensing elements from afferent vestibular and proprioceptive signals.
3. Compatible with prior manual-control models, e.g., those in Ref. 5.

Figure 3 details the assumed pilot model structure and forms for the Visual and Motion paths of Fig. 2. The rate and displacement elements in the "VISUAL PROCESSES" group are used to generate a lead time constant ($T_L = KR/K_D$) which pilots typically adopt to cancel the roll-subsidence mode in the controlled element (Ref. 3). The "integral" term is sometimes needed to represent the pilot's trimming actions and other low frequency behavior. (e.g., the so called "α-effects" in the Extended Crossover Model of Ref. 5)



ORIGINAL PAGE IS
OF POOR QUALITY

Figure 3. Assumed Pilot Model for Roll-Only Tracking

The extra visual time delays account for retinal and central (e.g., rate) processing as well as computational and display lags.

The tilt, velocity and acceleration terms in the "MOTION PROCESSES" are the simplest possible descriptors of the pilot's use of physical bank angle. These are not intended to represent motion sensors directly although the velocity term is very similar to the output of the semicircular canals over the forcing function frequency region. The tilt angle cue K_T is actually due to the lateral specific force due to the tilted g-vector.

The "ACTUATION PROCESSES" include a time delay and a third order neuromuscular system, the latter readily simplified to a second or even a first order approximation, as noted in the figure (e.g., for a second-order system set $T_N = 0$, whence $A_3 = 0$, $A_2 = 1/\omega_N^2$ and $A_1 = 2\zeta_N/\omega_N$). The delay terms τ_V and τ_M were actually modeled as first-order Pade polynomials, and by breaking up the net delays into two small portions the Pade roots (at $2/\tau$) are at sufficiently high frequency to give an excellent fit up to over 10 rad/sec.

Identification. — The two "opened-loop" expressions in Eq. 4a can be used to identify the two unknown paths (Visual and Motion) only if the Target and Disturbance inputs are independent. For signals constructed as a sum of sine waves this means that there can be no common frequencies. However this precludes the direct solution for the unknowns (V and M) since the "opened loop" expressions cannot be evaluated at the same frequencies. This dilemma was dealt with in Refs. 1 and 2 by linearly interpolating the measurements at the interleaved frequencies. This can lead to difficulties and inaccuracies in the vicinity of lightly damped modes, where the transfer functions are not smooth. A different technique is used where specific model forms are assumed for the Visual and Motion paths and the equations of motion are written for all elements and loops, so that in effect the "interpolations" are made with appropriately shaped math models. The unknown parameters are then adjusted by the STI Model Fitting Program (MFP; described below) so as to fit simultaneously the closed loop error and stick describing function responses to the Target and Disturbance inputs.

The STI Model Fitting Program was developed to fit high order multiloop models to frequency domain data (e.g., from Fast Fourier transforms and is described in Ref. 7. It evaluates selected transfer functions from fixed-form adjustable-parameter equations-of-motion written in a special way such that each adjustable parameter appears only once in the "matrix-of-equations." Thus, the influence of each parameter on any system response to any input is available. The program minimizes the vector difference between model and data transfer function responses using a variety of steepest descent techniques to minimize a cost function. This cost function is evaluated by squaring and amplitude weighting the difference in the real and imaginary parts of the data and model responses. In the present case, five frequencies of the task error-to-disturbance, four of the stick-to-disturbance and five of a linear sum of error- and stick-to-target were fit. The amplitude-weighting was the inverse of the data magnitude, thus each frequency was uniformly represented except that the highest frequency of the stick-to-disturbance was weighted 10 dB less.

Since the target and disturbance are sums of sinusoids, the effective "opened-loop" expressions in Eq. 4 were estimated using ratios of Fourier coefficients:

$$\hat{G}_I(j\omega) \Big|_I = \frac{\Phi}{E} = \left(\frac{PLNT}{VERR} \right) \text{ at Target frequencies, } \omega_I \quad (5)$$

$$\hat{G}_D(j\omega) \Big|_D = \frac{-C}{C_e} = \left(\frac{-STIK}{SERR} \right) \text{ at Disturbance frequencies, } \omega_D \quad (6)$$

where the four character names PLNT, VERR, STIK and SERR are defined in Fig. 1 and will be used to identify various responses in the remainder of this report.

To check the accuracy of this procedure an analog "autopilot" operation on both task error and measured motion was mechanized on the DES setup and the recorded signals were processed thru MFP. Table 3 summarizes the results of

TABLE 3. ORIGINAL AND RECOVERED PARAMETERS
FOR DUAL AUTOPILOT

$$\text{Visual Path: } V = \frac{K_R s + K_D}{T_V s + 1} e^{-\tau_V s}$$

$$\text{Motion Path: } IM = \frac{K_V s + K_T}{T_M s + 1}$$

CASE	"VISUAL LOOP"				"MOTION LOOP"		
	K_D	K_R	T_V	τ_V	K_T	K_V	T_M
Original	.133	.067	.100	.018	.040	.100	.100
Recovered by MFP	.134	.062	.098	.023	.040	.104	.092

this check, using the forms indicated. The time delay shown is an approximation to the net phase effects of various hybrid computation delays and high-frequency anti-aliasing filter lags. Some errors could be due to the fact that the "dialed-in" computer settings did not accurately represent the effective parameters. Generally the recovered parameters in Table 3 are quite close to the nominal, such that a transfer function plotted from the recovered parameters would be indistinguishable from one plotted for the original parameters.

Washout Dynamics

In addition to the static (no motion) case ("ST"), and full-motion cases with roll axis at 0 deg inclination "FO", and nose up 90 degrees, "F90"; four different washout schemes were tested:

- Purely Attenuated, "A" wherein the plant motions at all frequencies were multiplied by 1/2 in commanding the DES.
- First-Order, "W1"; where the low frequency motions are attenuated by a first-order high pass filter of the form:

$$\left. \frac{\Phi_M}{\Phi} \right|_{W1} = \frac{K_{hi} s}{s + 1/T} \quad (7)$$

where

K_{hi} = high frequency gain (near 1.0)

T = time constant ("break frequency" = $1/T$)

With this washout a step bank angle command returns experimentally to zero with a time constant of T sec.

- First-Order, Attenuated, "W1,A"; a combination of the two foregoing washouts, with different gains and break frequencies.
- Second-Order "W2"; the low frequency terms are washed out by second order high pass filter of the form

$$\left. \frac{\Phi_M}{\Phi} \right|_{W2} = \frac{K_{hi} s^2}{s^2 + 2\zeta\omega s + \omega^2} \quad (8)$$

where

ω = the break frequency, and

ζ = the damping ratio (typically .7)

With such a second-order washout an initial step bank angle returns with minimal overshoot with an effective delay (to half amplitude) of $(2\zeta/\omega)$ seconds. A constant roll rate input still ends up at zero bank angle.

The various washout parameters were originally selected to produce a reduction in rms roll amplitude to about 50 percent of the full motion case, based on a more-or-less arbitrary a priori assumption of a typical, invariant, second-order closed-loop pilot-simulator response to roll commands, characterized by a bandwidth of 3.6 rad/sec and a closed-loop damping ratio of $\zeta_{CL} = 0.6$. It was realized that in practice the pilot might change his response characteristics for different washouts, but this procedure was used to select the different parameters on a more rational basis than (say) fixed break frequencies of all the washouts.

In the simulation, inadvertent problems with mechanization of the filters and DES response properties slightly modified the intended wash-out dynamics. The actual response properties of the washout plus DES combination were fitted by the appropriate forms of Eqs. 7 and 8 and the effective washout-filter parameters were extracted. These are summarized in Table 4. Most of the effective parameters were close to the intended ones, except for the W2 high frequency gain which was 1.2 instead of the 1.0 desired. In Table 4 the cases are arranged in order of decreasing magnitude of rms physical roll angle, and this order will be used throughout the presentations to follow.

Measurements

A comprehensive set of measurements were made in an attempt to quantify all aspects of the pilot's performance, behavior, and effort.

TABLE 4. MOTION CONDITIONS AND WASHOUT DYNAMICS

Case:	F ₉₀	F ₀	W ₂	W ₁	W ₁ , A	A	ST
Washout Type:	"Full Motion" at 90°	"Full Motion" at 0°	"Second Order"	"First Order"	"First Order, Attenuated"	"Attenuated"	"Static"
High Frequency Gain	1.0	1.0	1.2	1.0	0.7	0.53	0
Break	—	—	$\omega = .85 \text{ r/s}$ $\zeta = .7$	1.0 r/s	.40 r/s	—	—

1. Performance Measures: Overall statistics (mean, variance, rms) of all signals, with emphasis herein on: tracking error stick force and physical roll-angle and rates.
2. Pilot Behavior Measures: Describing functions are the primary indicators of pilot behavior. The fitted parameters are useful for encoding efficiently the data, but the actual plots are often most informative. We use the "opened-loop" describing function, as they are the most useful and tie in with past experience on single loop systems.
3. Subjective Evaluations: Each subject was given a questionnaire about his tracking strategy, effects of motion cues and, differences due to washouts. Because these were not experienced pilots, no comparison to actual flight could be made; instead, subjects were asked to compare the motion cues with those of the F90 "real world" case.

APPARATUS AND PROCEDURES

Apparatus

The experiment was performed on the Dynamic Environmental Simulator (DES) at the Aerospace Medical Research Laboratory at Wright-Patterson Air Force Base. The DES is a man-rated centrifuge with independent roll and pitch cab control. For this experiment only the roll tracking motion was used, with the roll-rate limited to 90 deg/sec and the roll acceleration limited to 90 deg/sec². There are no limits on roll angle in the DES.

Within the cab, the subject seat was mounted such that the roll axis of rotation was roughly through the subject's head. Mounted on the seat was a right-side-mounted force stick for vehicle control. The elbow was braced, so that when the roll axis was 90 deg nose up, the hand was still comfortably over the stick. The cab contained a computer generated display, Fig. 4,

which was centered in azimuth a distance of approximately 17 inches from the subject's eyes. Subject's sitting height were such that the display was within 0 to 10 degrees of eye level. The "inside-out" display of target tracking error consisted of a 3.5 inch long rotating "target wing" whose center was superimposed upon a stationary horizontal dashed line nine inches in length. A .25 inch perpendicular "fin" at the center of the rotating line provided upright orientation.

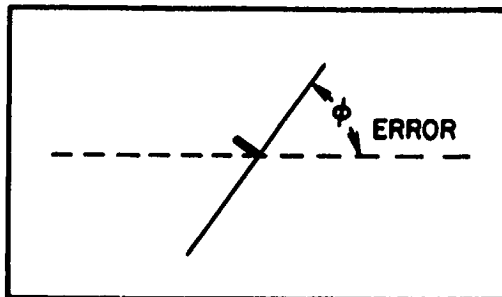


Figure 4. Sketch of the Roll Tracking Display

The DES is configured such that the pitch gimbal is outside of the roll gimbal. Thus it is possible to pitch the simulator nose up 90 degrees without affecting the roll axis tracking system. The cab pitched up 90 degrees was used for the "real-world" condition, as noted earlier.

Experimental Procedure

Four healthy college students between 18 and 25 years of age were used for the experiment. None were experienced pilots, so extensive training was necessary. Training was first accomplished for the static and two Full-Motion conditions. Tracking under each condition was considered one run. Each run lasted 165 sec and the three conditions or runs were presented in a random order each day. At the end of each run, subjects were presented their mean-squared-error score for that run. Training continued for approximately three weeks, three to six runs per day, at which time error scores began to reach asymptotic levels. Once performance leveled off, four more runs per subject per condition were performed and time history data was recorded for subsequent analysis.

For the second part of the study in which we investigated washout filter effects, we used the experimental design philosophy stated earlier — that washout filter effects should be compared to the "real-world" motion cues as encountered in the full motion no-tilt-cue case (F90). Therefore at the start of the evaluation of each washout filter, we let each subject first track in the F90 condition for one day. Following this we had each subject track normally (roll axis at 0 deg) with a given washout filter for three days, four runs per day. The last four runs for each subject with the washout filter were saved for data analysis. The procedure was followed for each washout filter investigated. As in the first part of the study, subjects were told their scores for motivational purposes.

Data Collection

A hybrid computer system was used for: display generation, forcing function creation, on-line error score computation, and time history data collection. From the time history data, root-mean-squared values and Fast Fourier Transforms (FFT) of each time signal were computed. From the FFT's power spectral densities and opened-loop describing functions (e.g., Eqs. 7 and 8) were computed. The frequency response data reduction, based upon the sum of sine waves generation, was similar to that employed in a preceding study (Ref. 3).

Comparisons among individual data showed good consistency, once sufficient training had occurred. Therefore, for each motion condition, the last four runs of every subject were averaged (16 runs total) by AMRL to give mean \pm standard deviation values for model fitting by STI. It is these averaged data that are analyzed in the following section on Results.

RESULTS

Limited space precludes the presentation, here, of all the reduced and averaged data. Instead we present typical time histories for one subject, averaged spectra and describing functions for a typical motion case, and then, after demonstrating that the fitted transfer functions truly represent the data, we present the "opened-loop" curves for various cases, and analyze the resulting performance and behavioral measures to answer the questions in the Introduction.

Typical Time History

A pair of time-histories of the various inputs and outputs for corresponding segments of static and full-motion runs, is given in Fig. 5. For these plots, identical target and disturbance inputs (top and bottom traces) were used in each run, to reveal the differences more clearly. The following features of the time histories should be noted:

- The disturbance input, which is summed downstream of the stick (and shown to the same scale) is effectively integrated by the vehicle dynamics to yield roll motions comparable in amplitude and frequency to the target input.
- In the static case the roll angle does not follow the target very well, because of these simultaneous, large disturbance inputs.
- Comparison of the E and C traces for the static case (where only the visually displayed error can be used) shows that the pilot is using both error displacement and rate in his compensating control actions.

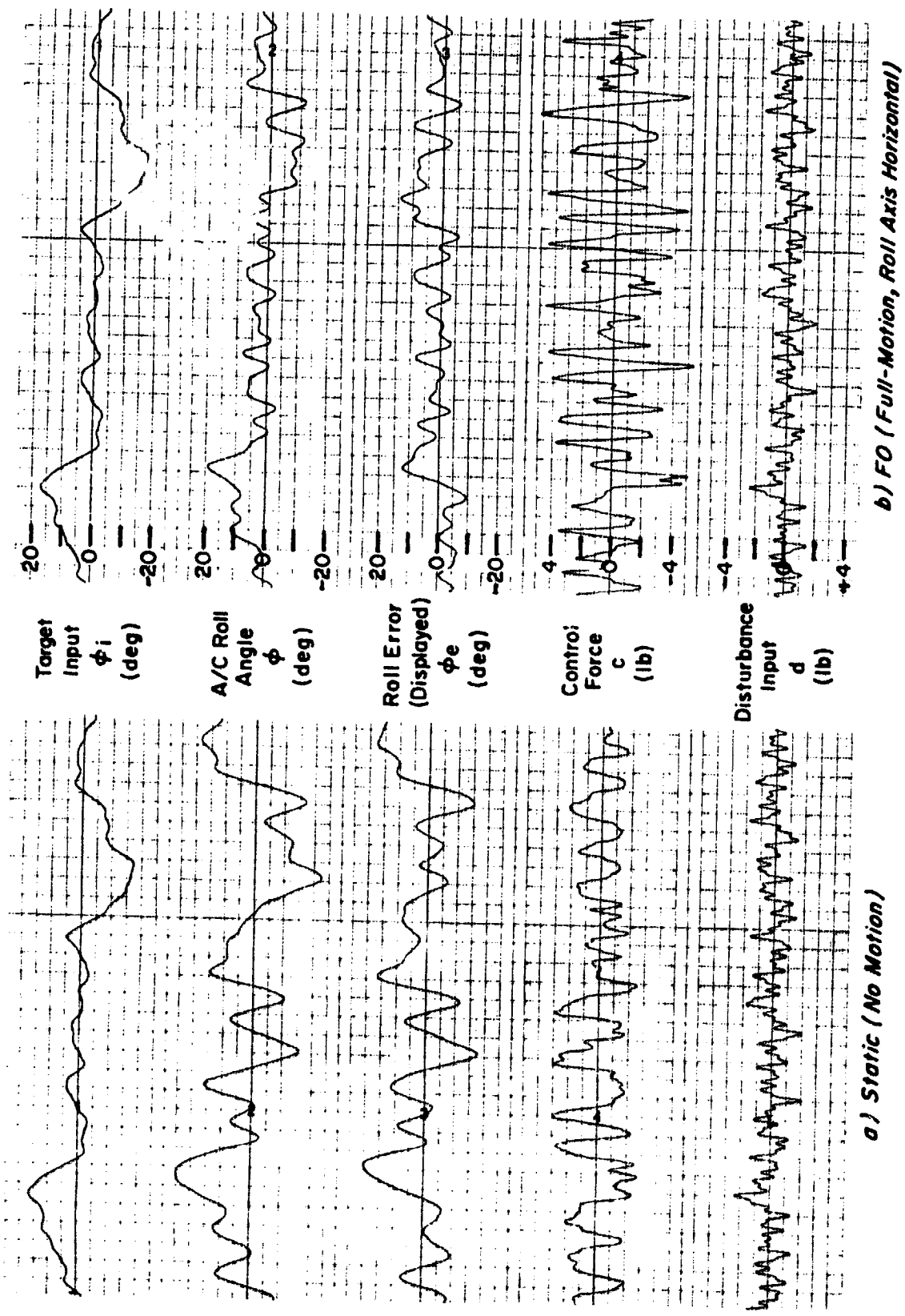


Figure 5. Typical Time Histories with No- and Full-Motion

ORIGINAL PAGE IS
OF POOR QUALITY

- Comparing the motion case to the static case, the control response is obviously a more aggressive and higher bandwidth (due to motion cues), while the tracking error is reduced.
- (Not shown) There is a remarkable consistency in the ϕ , E and C traces for repeated portions of the same inputs, showing a highly input-coherent and consistent operator response, as will be shown by the reduced data, later.

Frequency-Domain Data

Examination of the individual error scores and closed-loop describing functions showed that each of the subjects adopted similar behavior and so the results could be validly averaged, without loss of significant details in the average. Thus, approximately four runs each of four subjects were averaged for the data shown (a few runs were dropped due to data problems). The data shown here for the Full Motion Case with roll axis at 0 degrees (FO) is genuinely typical of all the cases investigated and was not selected as the best-examples available.

Spectra. — Figure 6 shows power spectra for the control stick, displayed error, and aircraft bank angle. The remnant shown (plotted at forcing function frequencies by the X symbols) is actually an average over neighboring (non-overlapping) estimates. The small standard deviations shown for all signal components indicate that all subjects had essentially the same, low variability, behavior. The signal-to-noise ratio is quite good at all but the very highest frequencies and implies a high coherency between the two inputs and responses. This permits the major part of the responses to be described by linearized describing functions. Notice that the spectrum of ϕ_{plant} (+) is large at low target frequencies (to follow the target) while its spectrum at low disturbance frequencies (\diamond) is lower, as desired.

Closed-Loop Describing Functions. — Figure 7 illustrates typical closed-loop describing function data (to which the model was fitted by the MFP procedure described earlier) for the control stick and task error responses to target and disturbance inputs. The frequencies used in the model fits are indicated by the arrows labeled "Fitted Freqs". Not all data points were used for computational economy. A preliminary analysis indicated that the selected frequency response points were the most sensitive indicators of pilot behavior.

Generally, the closed-loop data exhibit very low variability and the model fits capture every nuance of all the responses, using one set of model parameters and the various closed-loop relationships (e.g., in Fig. 2). The wiggles in the describing functions due to various low-damped modes, would greatly complicate simple interpolations between target frequencies to obtain vectors at disturbance frequencies, as done by earlier investigators (Refs. 1,5).

Model Fits. — Table 5 summarizes the model parameters fit to the data for all dual-input cases. Only nine of the twelve parameters in Fig. 3 were

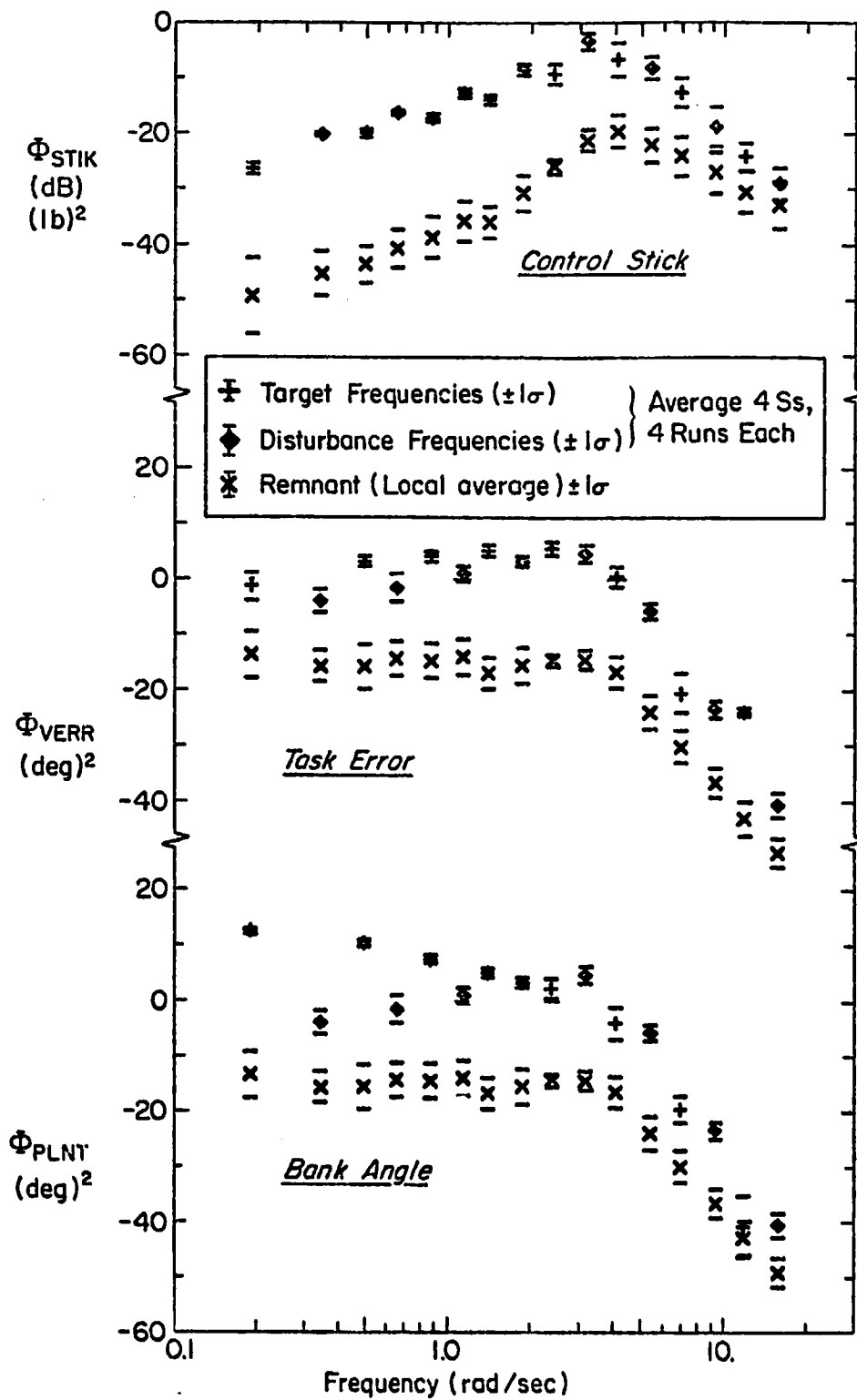
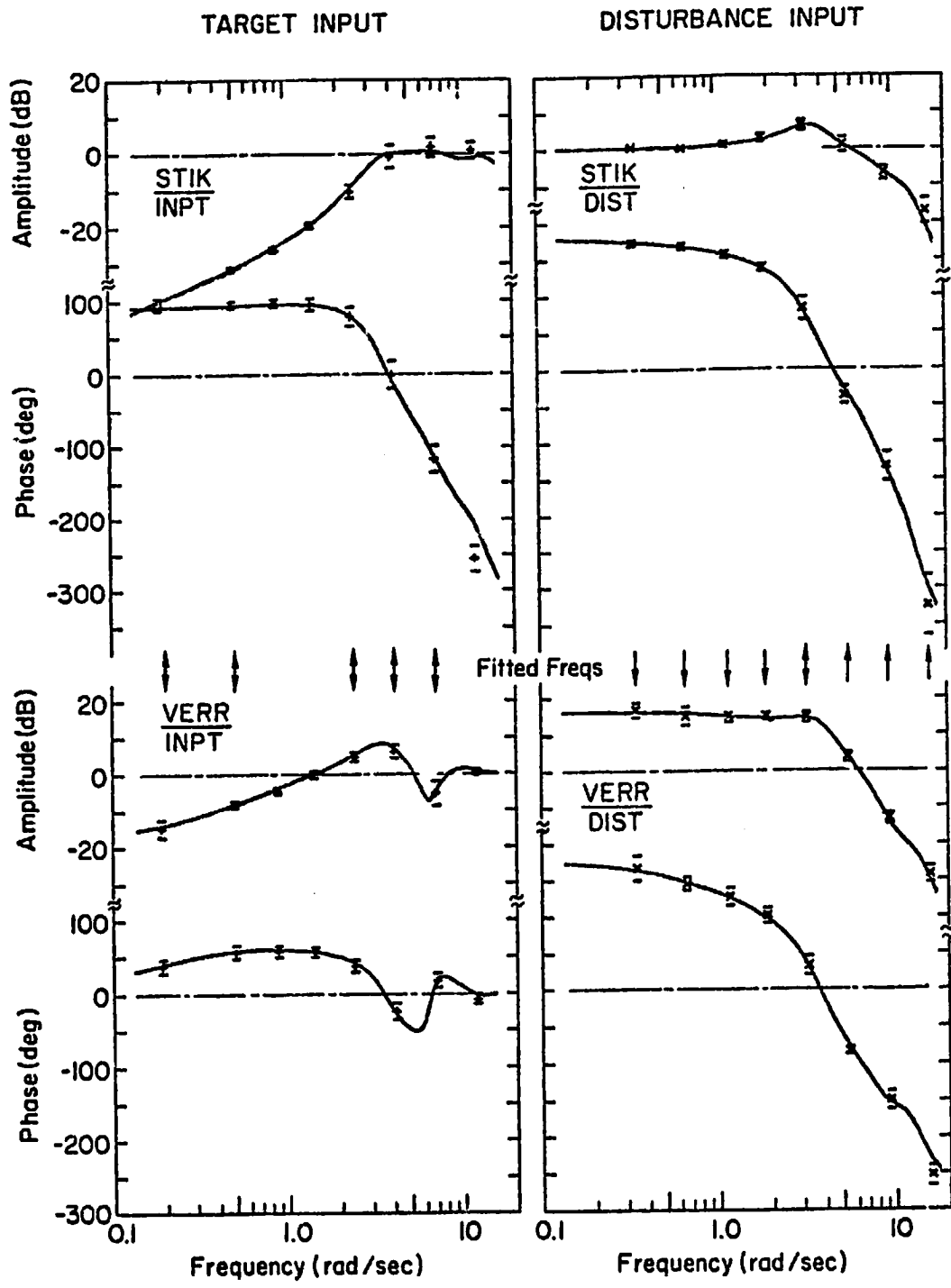


Figure 6. Typical Power Spectra for Full Motion, Erect (Case F0)



±	Target Input Data ($\pm 1\sigma$)	} Average 4 Ss, 4 Runs Each
±	Disturbance Input Data ($\pm 1\sigma$)	
—	Model Fits	

ORIGINAL PAGE IS
OF POOR QUALITY

Figure 7. Typical Closed Loop Describing Function Data and Model Fits for Full Motion, Erect (Dual Input, Case F0)

TABLE 5. SUMMARY OF MODEL PARAMETERS FIT TO DATA

CASE Motion Condition	MODEL PARAMETERS													REMARKS
	Visual						Motion			Neuromuscular				
	K_D lb/deg	K_R lb/deg/s	τ_V sec	$\frac{K_R}{K_D}$ sec	$\frac{K_R - \tau_V}{K_D}$ sec	K_T lb/deg	K_V lb/deg/s	K_A lb/deg/s ²	τ_M sec	ξ_N	ω_N rad/sec	$\tau_M A_1$ sec		
F90 Real World	0.149	0.068	0.16	0.46	0.30	-0.0001	0.076	0.020	0.15	0.26	9.3	0.20	Theor. $K_T \approx 0$	
F0 Full Motion	0.136	0.074	0.15	0.54	0.39	0.022	0.070	0.022	0.15	0.29	10.4	0.20	$\tau_M + A_1 =$ Effective Delay	
W2 2nd Washout	0.134	0.090	0.12	0.67	0.55	0.023	0.048	0.019	0.11	0.39	7.6	0.22		
W1 1st Washout	0.130	0.079	0.12	0.61	0.49	0.031	0.060	0.022	0.11	0.38	7.6	0.21		
W1, A 1st Wash + Atten.	0.119	0.070	0.08	0.59	0.51	0.040	0.081	0.031	0.17	0.28	9.0	0.23		
A Atten. Motion	0.122	0.053	0.06	0.43	0.37	0.056	0.131	0.028	0.15	0.13	8.2	0.19	$K_T, K_V \approx$ twice Values for F0	
ST Static	0.072	0.064	—	0.89	—	—	—	—	0.18	0.18	7.0	0.23		

(K_1, P_1, A_3 set to 0)

needed, as preliminary fits showed that a second order fit was sufficient for the neuromuscular mode ($T_N = 0$) and there appeared to be no error integrating action ($K_I = P_I = 0$). Lack of K_I and P_I (the so called α -effect in the Extended Crossover Model) may have been due to presence of the tilt cue in the motion cases with roll axis at 0 deg, but its absence at F90 and Static conditions is unusual.

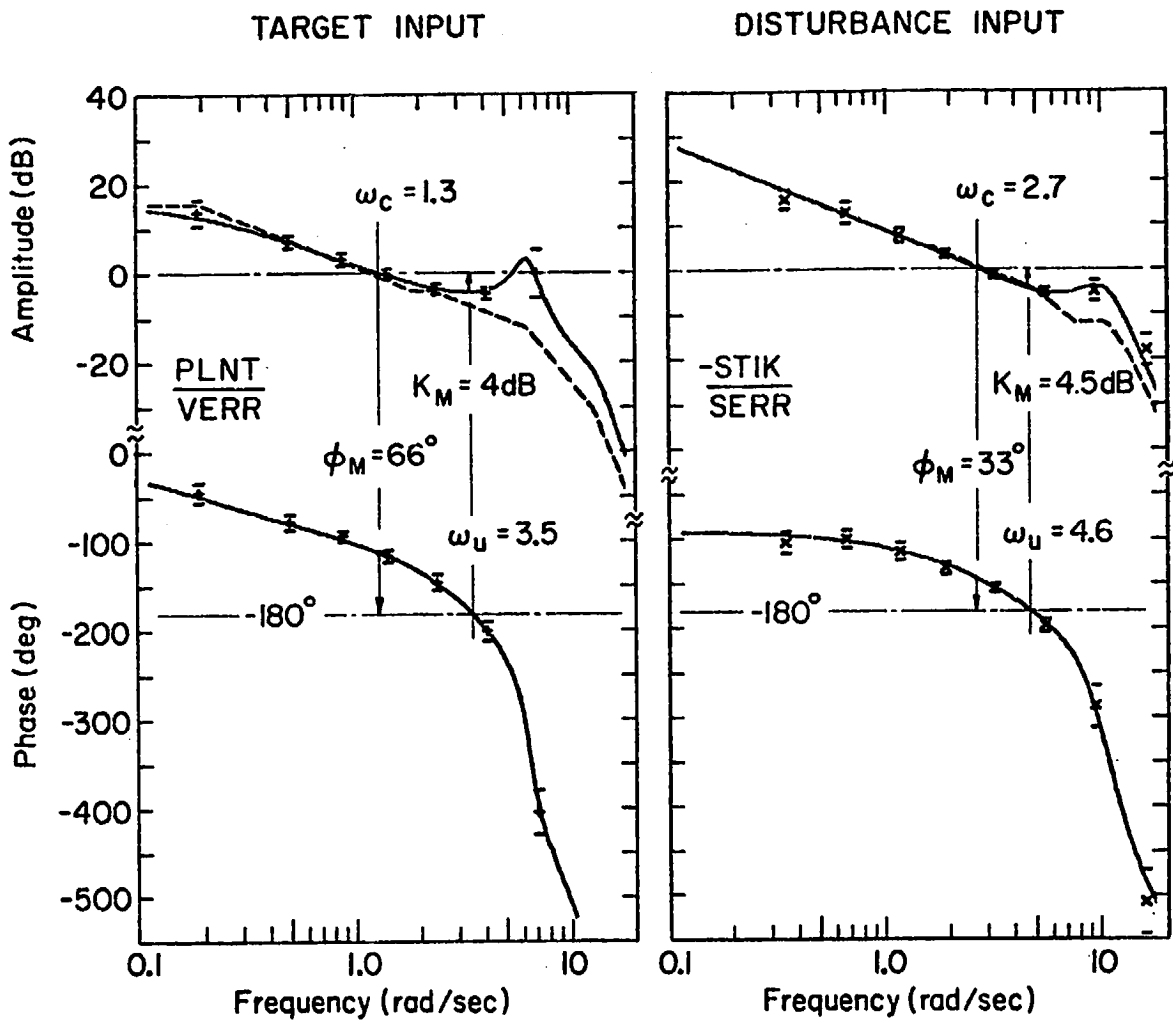
The additional columns in Table 5 detail the effective lead time constant in the visual path ($T_L = K_R/K_D$) and the effective time delay in the neuromuscular path ($\tau_e = \tau_M + A_1$). Note that the visual displacement gain, K_D , nearly doubles when going from Static to any Motion condition, and the tilt sensitivity, K_T , is negligible for the F90 case, as it should be, since no tilt cue is available.

Opened-Loop Describing Functions. — A number of other trends and covariations among parameters are evident; however, these effects can best be illustrated by using the "opened-loop" responses calculated using the measured closed-loop data along with the loop structure of Fig. 2 or the parameters in Table 5 with the model of Figs. 2 and 3. Figure 8 shows the resulting "opened-loop" data and computed model curve for the Full Motion, FO Case. As with the closed loop responses the model curve fits the actual "opened-loop" data very well — it truly represents the data. These data and fits for this example are typical; i.e., the other cases show effects similar in kind, differing only in degree. Thus, comparisons among cases can be made using the curve fits, as we will do in the remainder of this paper.

These multiple "opened-loop" describing functions have all of the appearance and significance of single open-loop transfer functions, and similar descriptive parameters apply. Some of these have been noted on Fig. 8, as defined below:

- ω_u = "unstable frequency" (180 deg phase crossover). This sets the maximum bandwidth of the loop, and is the frequency at which oscillations set in if the gain were further increased by K_M dB.
- ω_c = "crossover frequency" (0 dB gain crossover). This sets the effective bandwidth of the loop, and determines the resulting stability margins.
- K_M = "gain margin" — allowable gain increase for incipient loop instability.
- ϕ_M = "phase margin" — allowable phase lag for incipient loop instability.

In Fig. 8, it is apparent that the disturbance loop (dominated by the motion pathway) has a higher bandwidth and lower phase margin than the target loop (dominated by the visual pathway). This implies lower tracking errors, as will be shown later.



\bar{x}	Target Input Data ($\pm 1\sigma$)	} Average 4 Ss, 4 Runs Each
\bar{x}	Disturbance Input Data ($\pm 1\sigma$)	
—	Model Fits	
- - -	Model Asymptotes	

Figure 8. Typical Effective "Opened Loop" Data and Model Curve for Full Motion, Erect (Dual Input, Case FO)

The kinks in the dashed "asymptotes" in Fig. 8 show the poles (break downwards) and zeroes (break upward) of the model. The need for the relatively high order pilot-vehicle model used here is clearly shown by the spread between the asymptote breaks and the model fits as well as the different asymptotes in each "opened-loop."

Effects of Full Motion vs. Static Conditions

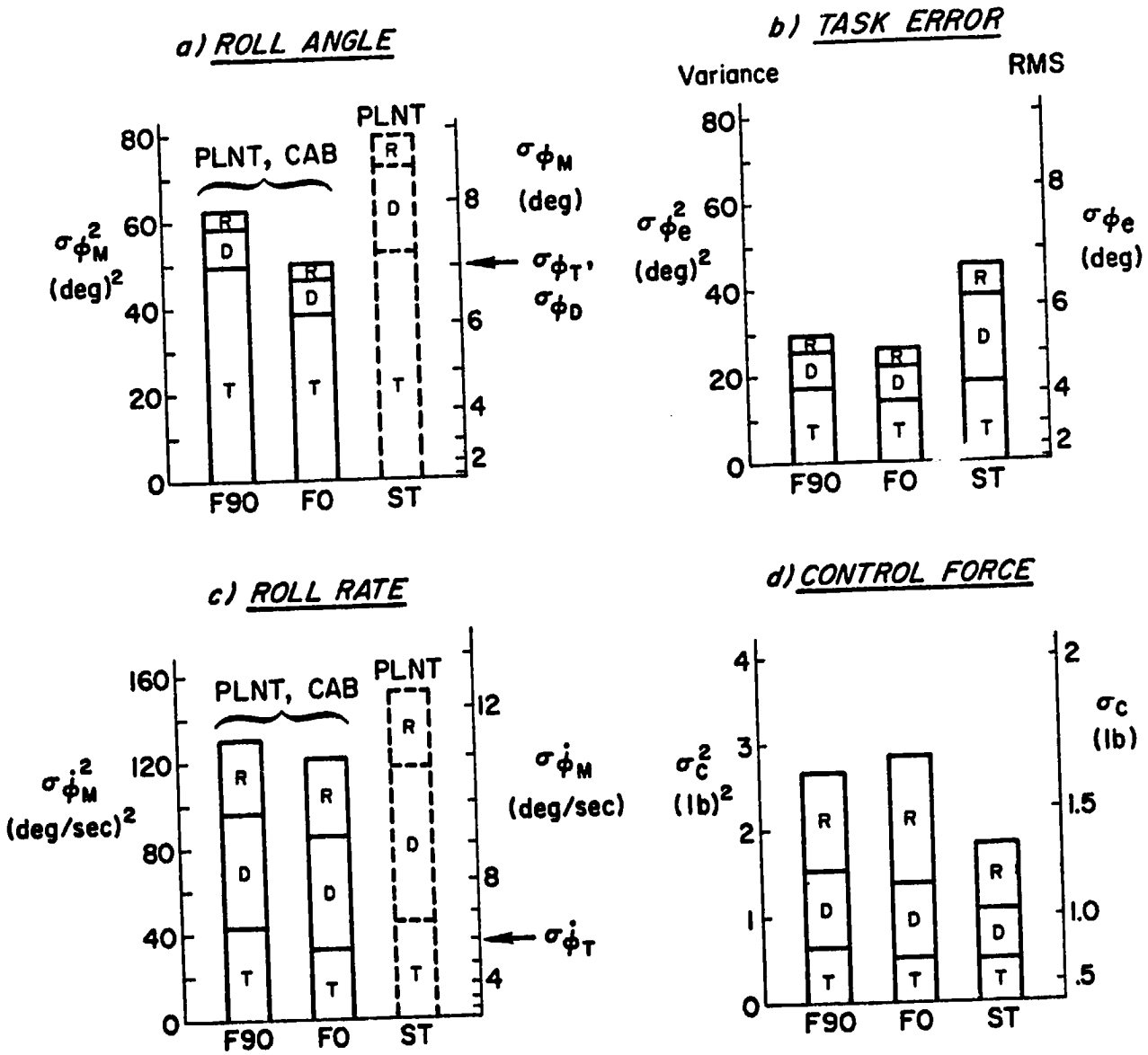
Figure 9 compares various performance measures for Full Motion and Static cases. Variances are used because they can be partitioned into summable vector components due to: Target, Disturbance and Remnant. Concentrating on task error, Fig. 9b, for the STATIC Case, the error components from Disturbance (D) and Target (T) inputs are essentially the same, reflecting the dual input spectrum design objective mentioned earlier. For the Full Motion at 90 deg (F90) case the target errors (T) are the same as for a Static cab, while the disturbance errors (D) are much smaller. Going from Full Motion, at 90 deg to the 0 deg (FO) case shows that the target following errors (T) are reduced slightly while the disturbance errors are unchanged.

These basic trends in the tracking performance are explained by the changes in the opened-loop describing functions (DF) shown in Fig. 10. For the Target Input DFs the Supine and Static cases having no tilt cues show essentially the same DF (which results in the same target following errors) whereas the Erect case (with the maximum tilt cue) has a smaller target error. For the Disturbance Input DF both motion cases (FO, F90) have the same DF, which explains why their "D" components were the same in Figs. 9a, 9c, 9d. Furthermore, the "Rate Cue Effect" (lower loop lags leading to higher cross-over frequencies with motion) leads to the motion/static performance effects denoted by the arrows. Thus Figs. 9 and 10 show that the subjects used motion cues to improve performance in two main ways.

- The lower lags (and higher ω_n) permitted by the vestibular sensory-motor loop enables, in effect, a "roll-rate damper loop" to be closed by the pilot, thereby allowing a tighter disturbance regulation loop to be used by him (a loop gain increase of about $2.7/1.7 = 1.6$). Consequently, the disturbance variance is reduced significantly.
- The tilt-cue was used at low frequencies to provide a sense of zero reference and, thereby, to avoid drifts and overshoots, the effects showing up as a low frequency phase reduction on the target "opened-loop."

Components of the Multiloop Describing Function Under Motion

Further insight may be gained into the complexity of the multiloop interactions and motion effects via Fig. 11, in which the fitted model has been used, via the loop structure and equations of Fig. 2, to examine: each



Legend:
 F90 = Full Motion, Supine; FO = Full Motion, Erect; ST = Static
 Components due to: T = Target, D = Disturbance, R = Remnant
 Average of 4 Ss, 4 Runs Each

Figure 9. Effects of Full Motion (Supine, Erect) and Static Cases on Performance

ORIGINAL PAGE IS
OF POOR QUALITY

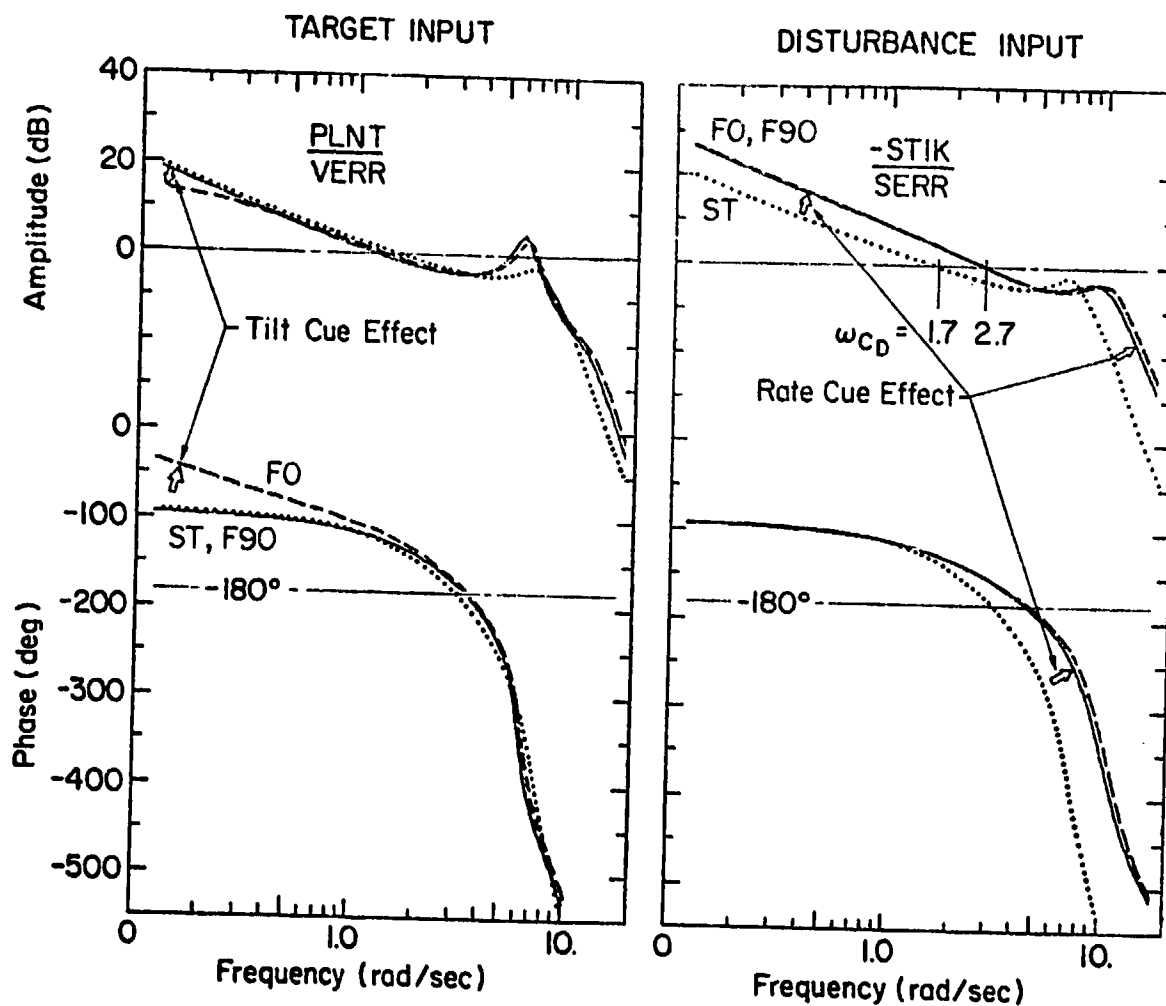


Figure 10. Effect of Motion Cues on "Opened Loop" Describing Functions (Dual Input Cases)

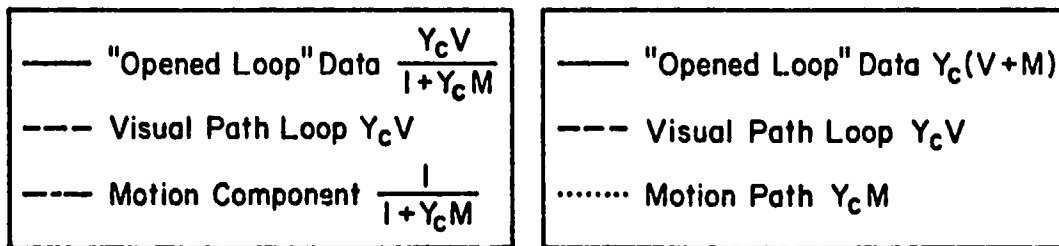
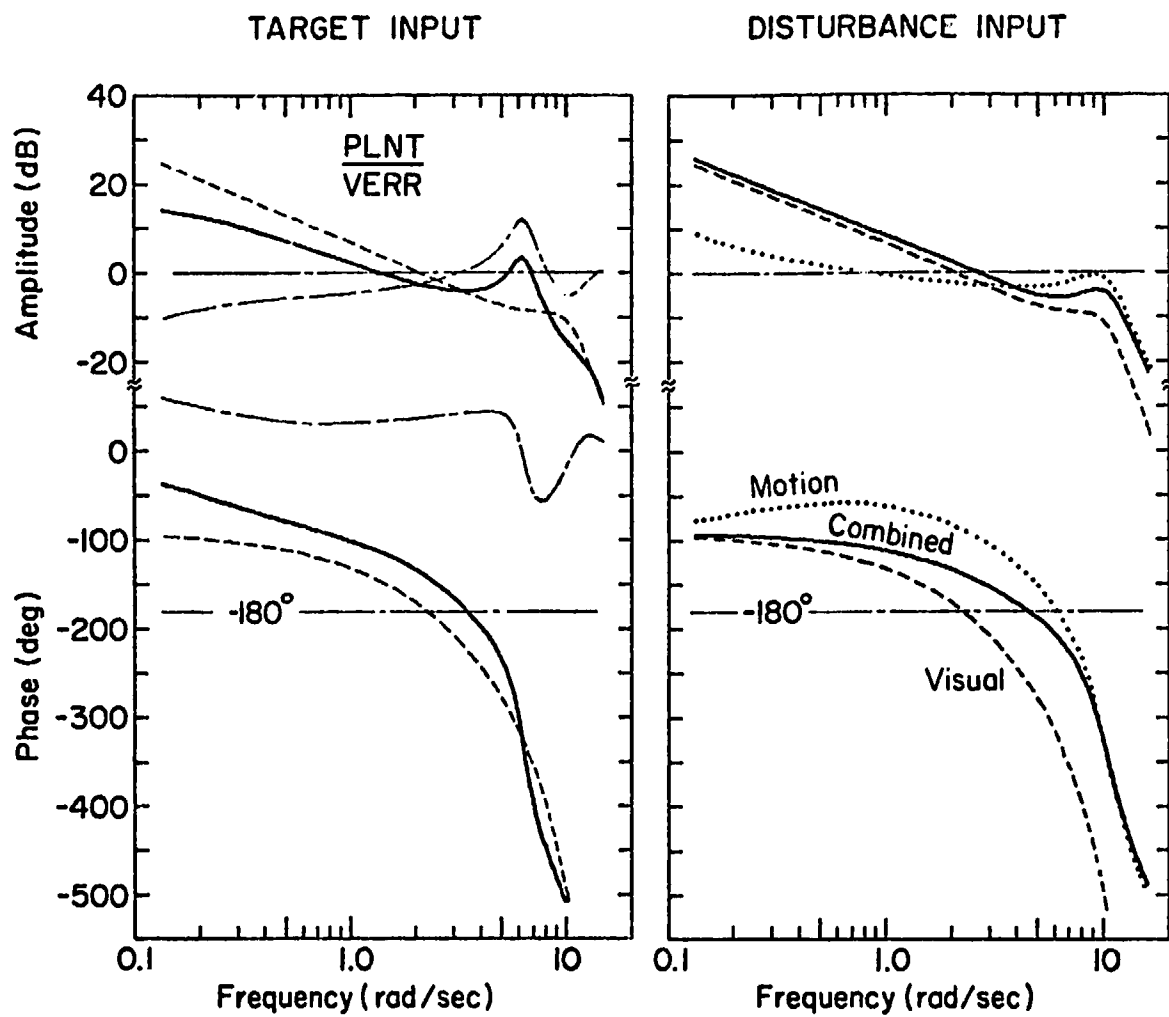


Figure 11. Behavioral Components of "Opened Loop" Data
(Dual Input, Full Motion Erect Case F0)

sensory loop individually (visual = dashed, motion = dotted) with the other simply turned off, and then the combined "opened-loop" (solid line) as discussed earlier in Section II-C. Remember that the "opened-loop" DF is a complex vector function of V and M, as noted in the legend.

Without going into details, the key points revealed by Fig. 11 are as follows:

- The Disturbance Input loop (on right) is a simple vector sum of VY_C and MY_C . The flat amplitude of the motion loop (dotted) shows that MY_C acts like a roll-rate feedback loop with an effective time delay, τ_e , appreciably less than the visual loop (for MY_C ; $\tau_e \doteq .20$ sec, for VY_C ; $\tau_e \doteq .20 + .15 = .35$ s). Over the important crossover frequency region of 0.5-5.0 r/s, their vector sum (solid) has an apparent τ_e even less than MY_C alone! This is consistent with and "explains" the results of Stapleford (Ref. 1) and Shirley (Ref. 2).
- At low frequencies the Disturbance regulation (solid) is dominated by (closest to) the visual loop at low frequencies and motion loop at high frequencies.
- The Target following loop (on the left) is a more complex function of VY_C and MY_C as seen in the equations in the box. (The motion component $(1 + Y_C M)^{-1}$ is shown dash-dotted to distinguish it from $Y_C M$ alone. Here, the solid curve is the vector product of the two components). In both amplitude and phase, the Target following loop dynamics are dominated by the visual loop (dashed) at all frequencies.
- A comparison (not shown here) of the purely visual static case per se (dotted curve of previous Fig. 10) and the isolated VY_C (dashed curve of Fig. 11) shows that they are not the same. When motion is present, the visual loop can be (and is) operated at higher gains, albeit with a slightly larger lead equalization (T_L) and consequently larger τ_e . (Per Table 5, $T_L \doteq 0.89$ sec and $\tau_e \doteq 0.23$ sec for the ST case; while $T_L = 0.54$ sec and $\tau_e = 0.20 + 0.15 = 0.35$ sec for the FC Case).

This analysis of Fig. 11, and others like it, clearly shows that one cannot simply add a motion feedback loop to the static case dynamics to get the combined result. Instead the operator optimizes his combined loop properties for the case at hand.

Effects of Single vs. Dual Forcing Functions

For some Full Motion cases (F90, F0), data were taken for Target input alone; and for Case F90, Disturbance input alone, to compare with the dual input case. When either input was used alone, it was increased by the square-root-of-two to keep the rms input the same as in the dual input case.

In general one might expect that if the disturbance alone were present, the pilot would adopt a different optimum behavior, because all he would have to do is to suppress both the felt and seen motions. Conversely, for the target alone, the pilot might more aggressively track the error, because the unseen disturbances were absent.

The results, shown in the opened-loop describing functions in Fig. 12, did not follow these expectations! For simplicity, the curve in Fig. 12 is that fitted to the corresponding dual input case, for which it passed precisely thru every data point on both sets of DF (e.g., see Fig. 8). The single-input data are shown relative to this dual-input curve in Fig. 12, remembering that each of the data plots represents a different set of runs. Somewhat to our surprise, the single input data are not significantly different from the dual input case, for the points generally lie within one symbol width of the curve and almost all lie well within ± 1 standard deviation of the dual-input curve.

How can this be, in the light of the theoretical expectations discussed above, considering that all pilots were given plenty of practice on every case, and noting that all behaved similarly (evidenced by the low scatter)?

Some hypotheses are:

- The "optimum" behavior was, perhaps fortuitously, nearly identical for the single and dual input cases. The combination of lightly damped modes in the controlled element near the neuromuscular modes plus stick lags has been identified as the so-called "Pilot Induced Oscillation Syndrome" of Ref. 8. These restrict the degree of equalization which can be used by the pilot to improve performance. Consequently, he may be operating near this constrained limit in all cases.
- The pilots were so overtrained in the dual case that they did not adapt "optimum" behavior in the single input cases despite plenty of practice with it. If so, this raises questions with respect to the assumption that pilots adopt an "optimum" behavior.
- There was some error in the experiment, such that dual inputs were really present. We checked this and verified that only the specified single input spectra and rms signals were present.

Here is an ideal, simple test case against which to validate the optimal adaptation models (e.g., Ref. 4). The inputs are analytically tractable, the good model fits show that the data are representable by linear, modest-order state equations, and the data are precise, have high signal-to-noise, and are internally self consistent. Such a validation remains as a future task.

Meanwhile, this result tentatively implies that the dual-input results should apply to the single input situations, if the inputs and controlled elements are similar to those used herein.

ORIGINAL PAGE IS
OF POOR QUALITY

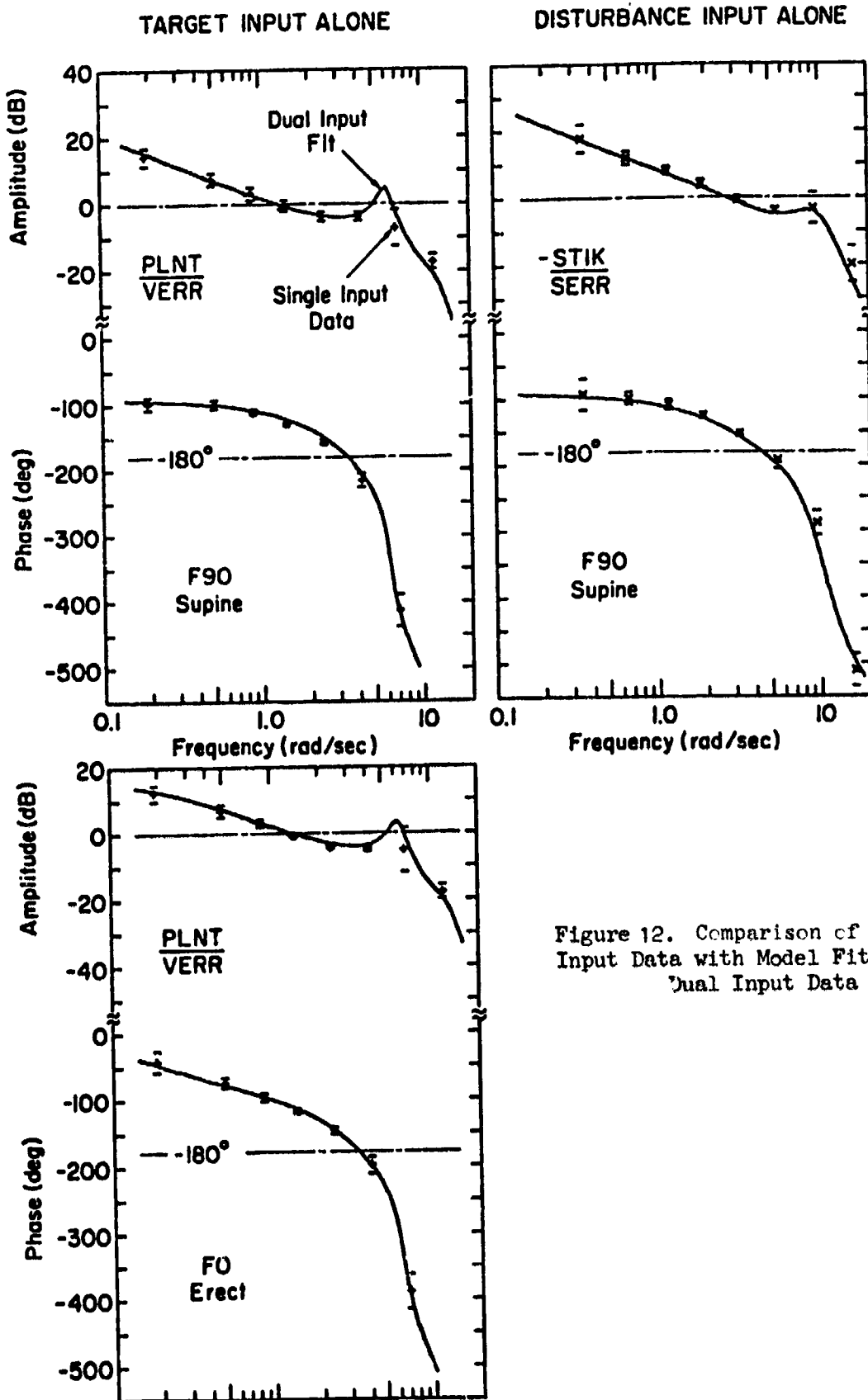


Figure 12. Comparison of Single Input Data with Model Fit from Dual Input Data

Effects of Motion Shaping (Washouts)

Having presented the results on our first question — that of basic motion effects vs. no motion, we turn now to the second question: What are the effects of various motion "shaping" (attenuations and/or washouts)? For this purpose, the data will be restricted to the dual-input cases, all with roll axis horizontal, i.e., FO, W2, W1, W1A, ATT, in the order of decreasing recovered roll angle.

Figure 13 shows various performance measures for these cases.² Consider first the variance of recovered (measured physical) roll angle, σ_{ϕ_M} , shown at the upper left, each case broken down in terms of the components due to target, disturbance and remnant. Noted on the margin are the variances for the target (or disturbance) alone, and their sum. Ideally, the recovered variance would consist of only the target component (equal to $\sigma_{\phi_T}^2$, attenuated by the motion shaping washout) and no disturbance or remnant portions. It may be recalled from Fig. 9 that in the (real-world) "F-90" case this ideal is approached, in that the target component nearly equals the commands, while the disturbance and remnant portions were small fractions of that.

With these standards in mind, let us consider the effects of various washouts. As described in Section II on Experimental Design, the overall scheme was to select different forms of motion washout, each selected (albeit crudely) to give the same attenuation of roll angle to about 50 percent of the basic, FO, case (i.e., the target roll variance of 1/4 of the basic level). As seen in Fig. 13a, this was achieved closely only for the pure attenuation case ($\sigma_{\phi_M} \approx 3.6$ deg vs. $\sigma_{\phi_T} \approx 7.0$ deg). The ATT computed roll motions (shown dashed) were nearly equal to the FO case, as were the other task performance measures in Fig. 13 (e.g., tracking error and control force) implying a close matching of the visual and motion-loop behavior in the basic and ATT cases, despite the lower magnitude of motion cues in the latter. (More on this later).

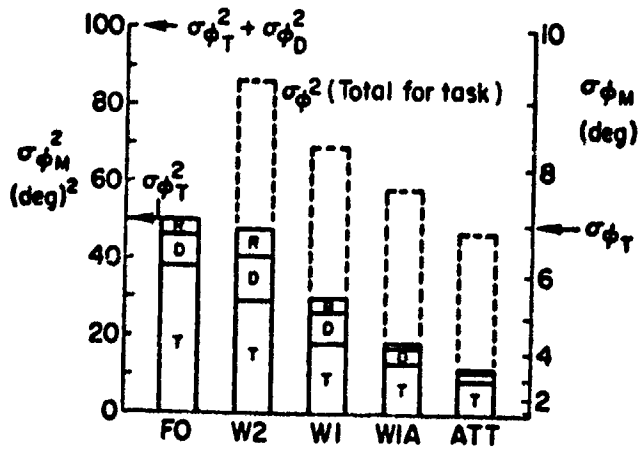
The Second Order Washout (W2) (which greatly attenuates the lowest frequencies) distorted the perceived motion cues (per the subjective questionnaire) and failed to reduce the motions as intended. Analysis of these results showed that this was due to the following reasons:

- a. The washout was a compromise design* such that the high-frequency asymptote magnified the roll angles (and rates) above the break frequency of .85 r/s by a factor of about 1.2, causing the roll rate variance (Fig. 13-c), and high frequency portions of the roll angle variance, to be increased by $(1.2)^2 = 1.4$ relative to the intended case.

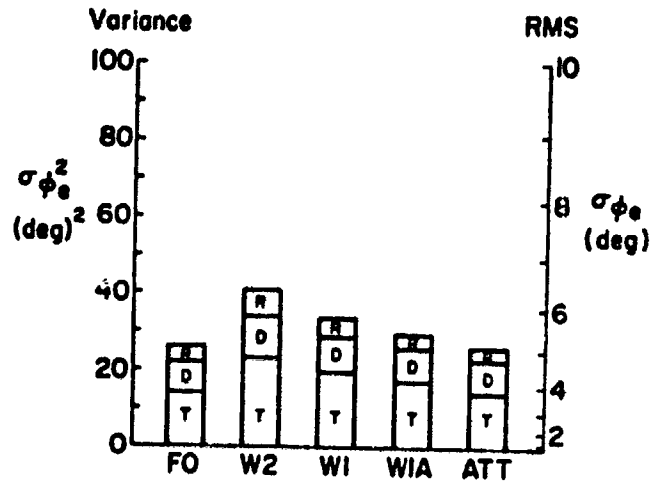
* The DES is a velocity system and as such would drift whenever a cascade washout was used. Consequently, a feedback scheme was devised that approximated the desired cascade washout but a perfect match at both high and low frequencies was not possible.

ORIGINAL PAGE IS
OF POOR QUALITY

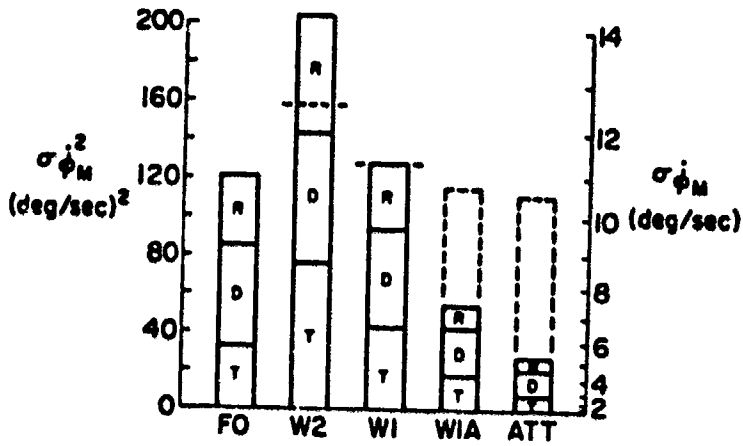
a) RECOVERED ROLL ANGLE



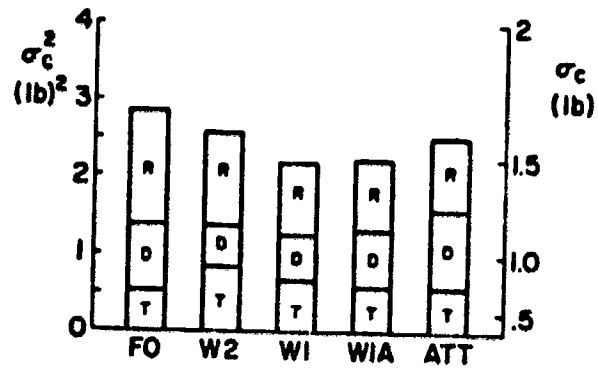
b) ROLL TRACKING ERROR



c) RECOVERED ROLL RATE



d) CONTROL FORCE



Legend:

FO = Full Motion, Erect; W2 = Second-Order Washout,
 W1 = First-Order Washout, WIA = First-Order Attenuated,
 ATT = Attenuated
 Components due to: T = Target, D = Disturbance, R = Remnant
 Average of 4 Ss, 4 Runs Each
 Solid = Recovered Motions; Dashed = Computed for Task

Figure 13. Effects of Motion Shaping on Performance

- b. The distortion of the felt motions relative to the visual motions caused the pilots to perform even worse than in the static case.

The other washouts were intermediate in recovered motion and plant motion between the Full and Attenuated cases.

Attenuation reduces both the recovered roll angles and roll rates in the same proportion, but washout reduces mainly the low frequency components and, thereby, reduces the roll rates less than the roll angles. This can be seen by comparing Figs. 13a vs. 13c for the W2 and W1 cases, especially.

Except for the anomalous W2 case, discussed above, the performance measures of tracking error and control force were not significantly different among any of the first order or attenuated wash out cases (See Figs. 13b and 13d). Even the proportions of each variance due to: target inputs, disturbances, and remnant were about the same as for the full motion case (FO).

Further insight into the pilot's tracking behavior under these washouts is given by the opened-loop describing functions in Fig. 14. It is immediately apparent that the disturbance-loop describing functions are nearly identical, implying the following:

- Despite attenuated, reduced-low-frequency motions, and phase distortions, the pilot compensated to give the same opened-loop DF.
- In the ATT case, the rms roll angle was reduced from 7 deg to 3.6 deg, the pilot had double his tilt and roll rate gains, (K_T , K_V) as verified by the fitted coefficients in Table 5, and summarized below:

Case:	σ_ϕ	K_T	K_V	K_A
FO	7°	.022	.070	.022
ATT	3.6°	.056	.131	.028
Ratio: (ATT/FO)	.51	2.55	1.87	1.27

Despite the fact that the rms tilt angle in the ATT case represents a lateral-specific-force cue of less than $3.6/57.3 = .063 \text{ g}_y$, the roll rates were apparently sufficiently high to be readily sensed and used to compensate for the reduced motion cue over the FO case.

On the left of Fig. 14 is the target-loop DF, where the following effects of washout are clearly apparent:

- the FO and ATT cases are nearly identical for the same reasons given above for the invariant disturbance loop DF.

ORIGINAL PAGE IS
OF POOR QUALITY

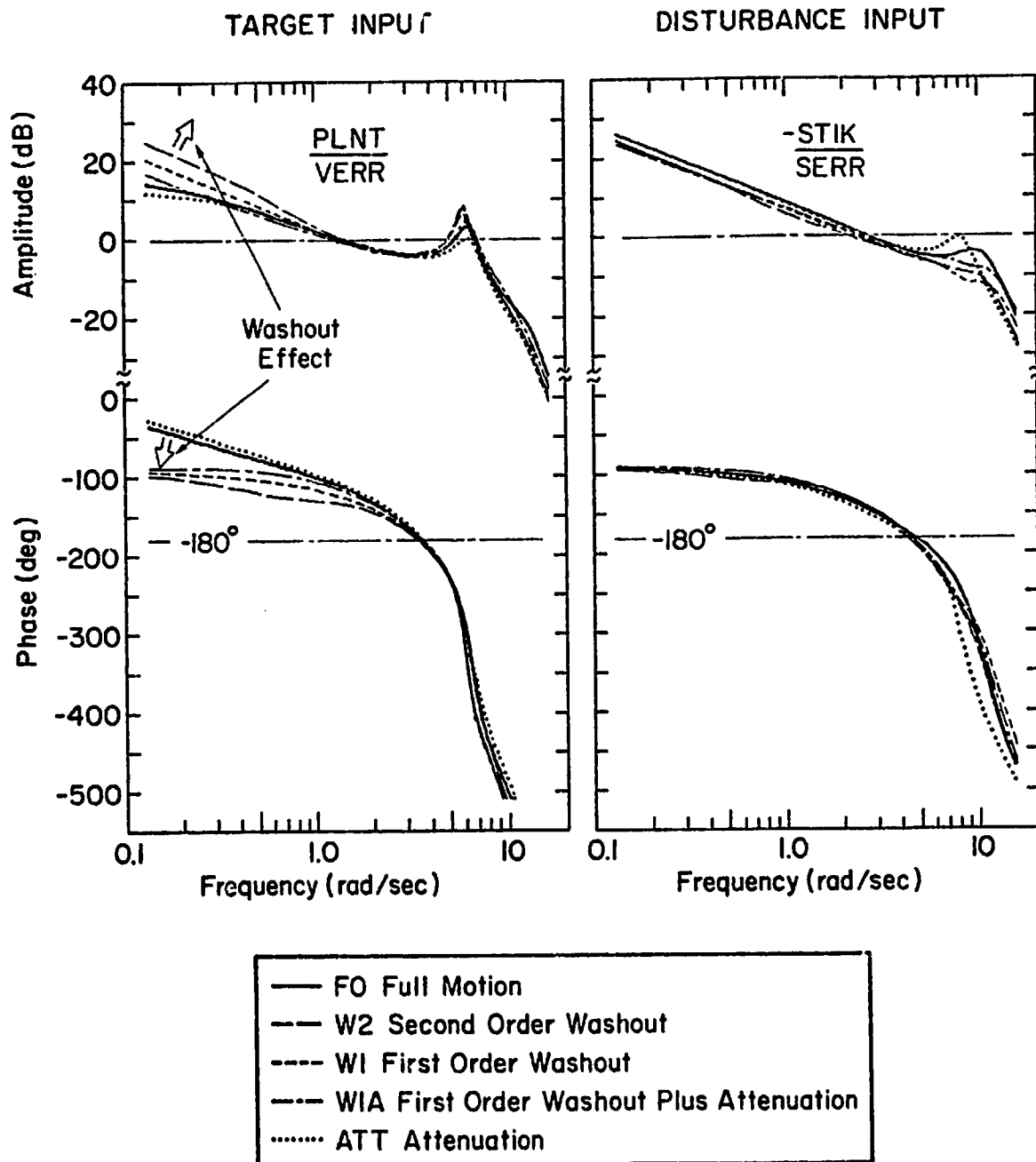


Figure 14. Effects of Motion Shaping for "Opened Loop" Describing Function (Dual Input Cases, Roll Axis Horizontal)

- the other washouts induce (at low frequencies) higher amplitude ratio and more phase lag as the washout degree is increased from ATT, to W2. An analysis indicates that these trends reflect fairly complex interactions similar to that of Fig. 11 (Left side). Note that inserting a low frequency washout to the motion path (M in Fig. 11) causes the resulting curve to start (at low frequencies) on the dashed curve and transition to the solid curve with increasing frequency. These amplitude and phase trends explain the "Washout Effect" in Fig. 14.

Optimum Washout

One of the objectives of this experiment was to find the optimum washout for AMRL's roll-only simulators. The desirable criteria are relative to the "real-world" case: a) significant reduction in roll amplitude and rates, and b) similar pilot behavior and performance.

Inspection of the foregoing results reveals that the clear choice is the first-order attenuated washout (W1A). Figure 15 justifies this selection based on the following comparisons with the F90 ("real-world" baseline) case:

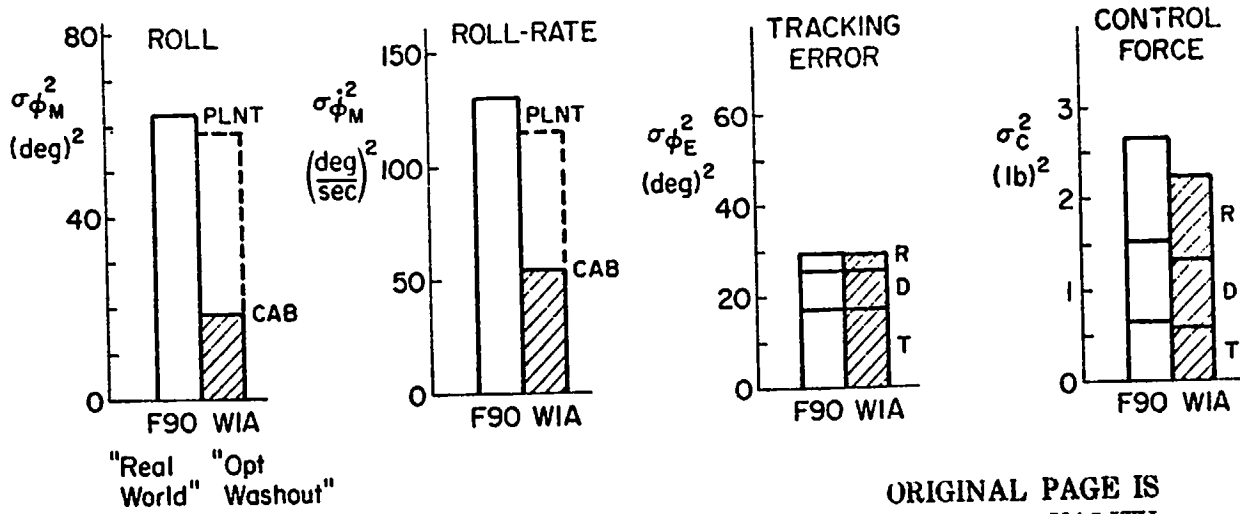
- Large reduction is recovered roll-angle and rate — as shown in Fig. 15a — with similar plant roll angles and rates.
- Very similar tracking error performance and control activity, as shown in Fig. 15b and 15c. Even the distributions of each variance from target, disturbance, and remnant inputs is closely matched.
- The opened-loop describing functions, shown in Fig. 15d, are practically identical. This is because the effect of tilt cue usage previously described in connection with Fig. 10, is almost exactly cancelled by the washout-break effect noted in Fig. 14.
- (Not shown) The subjective comments were more favorable for this washout than any other except pure attenuation.

Thus, we recommend first-order attenuated washout for use on all AMRL roll-only type simulators. The degree to which this form can be extended has not been determined, but the data suggest the following as likely to be both useful and satisfactory to pilots:

- Attenuation factor of 0.5 to 0.7
- Break frequency of 0.3+ to 0.5 rad/sec (Washout time-constant of 2-3 sec).

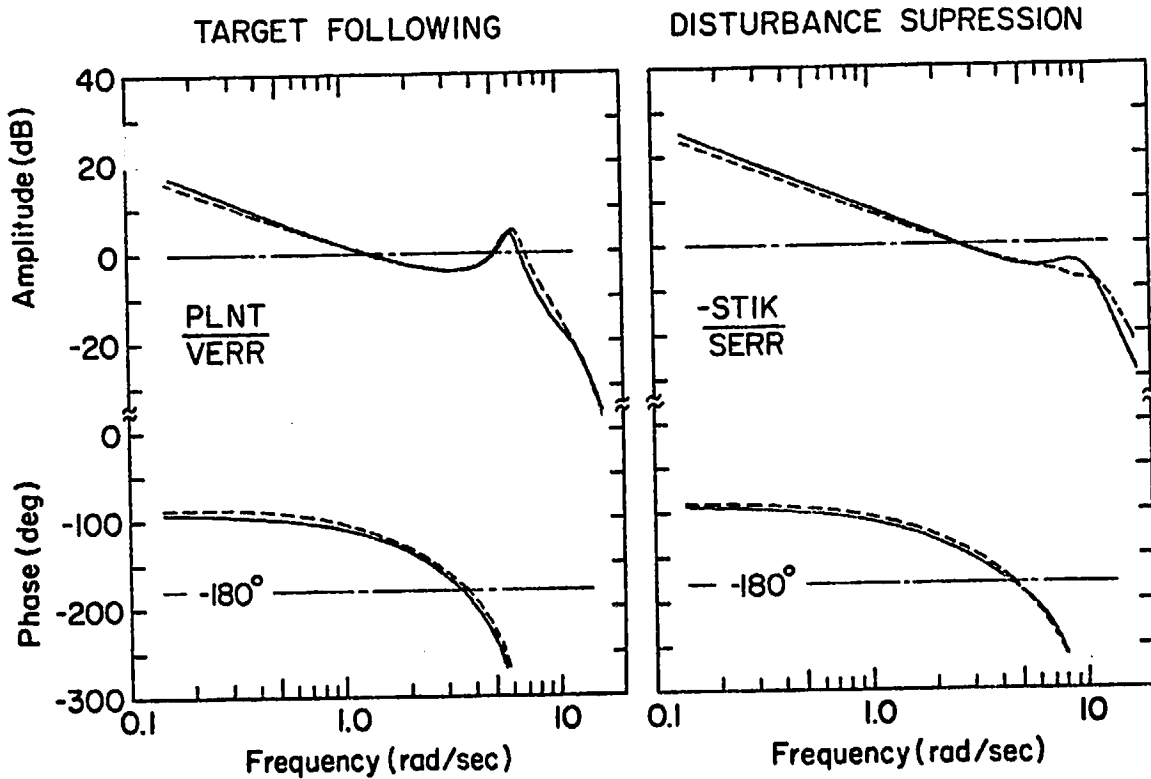
a) Cab Motions (Reduced)

b) Performance (Same) c) Activity (Same)



ORIGINAL PAGE IS OF POOR QUALITY

d) Pilot Dynamic Behavior (similar opened-loop descr. fcn.s.)



Motion Fit	Case	
————	F90	"Real World", Full Motion, Supine
-----	WIA	Optimum Washout (first order washout plus attenuation)
		1/T = 0.4 rad/sec, Attenuation = 0.7

Figure 15. Comparison of Optimum Washout with "Real World" Case

CONCLUSIONS

This research has covered several very well trained subject's responses to a variety of motion cases in a roll-only motion simulator, with simultaneous target and disturbance inputs. The results presented here support the following conclusions:

1. Across all seven conditions the four subjects were very consistent in their tracking behavior and scores, providing an exceptionally, reliable, and definitive data base worthy of detailed analysis, even beyond that performed herein (e.g., on remnant effects).
2. The multiloop model structure presented in Fig. 1, which has both visual, motion and (a common) neuromuscular dynamic elements, proved capable of accurately fitting the closed- and "opened"-loop describing functions at all measurable signal points within the loop. In combination with the interleaved sum-of-sinusoids target and disturbance inputs the new STI Multiloop Fitting Program (MFP) provided efficient fits of 10 parameters in a multiloop situation which had heretofore been very difficult to fit because of the complex interactions involved between the visual and motion feedback paths.
3. Untangling the closed-multiple loop describing function data in the "opened-loop" manner shown here provides a ready comparison with traditional single open-loop data. Similar effects (e.g., the Crossover-law adaptive behavior) are shown for the dual input case, with the disturbance loop having the higher bandwidth (limited mainly by the controlled element and vestibular rate-sensing dynamics).
4. After lots of analysis and digesting of complex trends in the various cases, the key to understanding it all seems to be the following:
 - Given reasonable rate motion cues at frequencies above about 0.5-1.0 rad/sec, the pilot's motion feedback system acts like an adaptive roll-rate damper with a bandwidth of nearly 3 rad/sec. This tends to suppress disturbances but opposes target following motions, while stabilizing both loops.
 - The pilot then uses sufficient extra visual compensatory (error correcting) gain to follow target commands as well under motion as in the static case, and with less remnant and disturbance components.

5. The affects of motion are consistent with the prior work of Stapleford (Ref. 1), Shirley (Ref. 2) and Levison *et al* (Ref. 4), while extending this work to the new case of equally strong target and disturbance inputs each having comparable apparent spectra at the display.
6. The describing functions and fitted tilt-cue parameter clearly showed that the spurious tilt cues from rolling with roll-axis horizontal are used, even though the rms lateral specific force was in some cases much less than 0.1 gy. A very simple model for the use of this cue is given. Nevertheless, use of this cue resulted in only small improvements in tracking performance in this random-input tracking task.
7. The four types of motion washout investigated (second-order, first-order, first-order-attenuated, and purely-attenuated) showed distinct effects compared to the "real-world" reference case of full motion about a vertical roll axis; the second-order case was the least desirable because of large differences in performance, behavior, (describing functions) and subjective ratings. The other cases provided roughly similar performance measures with some small differences in relative remnant, describing functions, and ratings.
8. The pilots clearly adapted differently to the various washouts, thus complicating the job of predicting the net effects for a given washout.
9. The optimum washout for roll-only-simulators (from the standpoint of performance, behavior and ratings similar to the "real-world" reference case) was clearly the first-order, attenuated washout. Recommended parameters (for this type of task) would be: attenuation factor 0.5-0.7, and washout time-constant of 2-3 seconds (break at 0.3-0.5 rad/sec).

The data base for this paper is being prepared for permanent filing and general access at the U.S. Defense Documentation Center (DDC); and may be requested through the third author, at AMRL.

It would be interesting and fruitful to analyze and model the remnant portion of these data, using the closed-loop spectral data available (e.g., as in Fig. 6). Because the inputs were carefully selected and shaped to be representable by filtered white noise, various optimal-control-theories could be tested against this very consistent, accurate, and definitive data base. Finally, using these model and parameters (which precisely fit almost every data point,) various analytical manipulations of the data can be performed to gain further insight about pilot adaptation to motion cues and washouts.

REFERENCES

1. Stapleford, Robert L., Richard A. Peters, and Fred R. Alex, Experiments and a Model for Pilot Dynamics with Visual and Motion Inputs, NASA CR-1325, May 1969.
2. Shirley, R. S., "Motion Cues in Man-Vehicle Control," M.I.T., Cambridge, MA, Sc.D. Thesis, Jan. 1968.
3. Levison, W. H., S. Baron, and A. M. Junker, Modeling the Effects of Environmental Factors on Human Control and Information Processing, AMRL-TR-76-74, Aerospace Medical Research Laboratory, Wright-Patterson AFB, Ohio, Aug. 1976.
4. Levison, W. H. and A. M. Junker, A Model for the Pilot's Use of Motion Cues in Roll-Axis Tracking Tasks, Bolt Beranek and Newman, Inc., Cambridge, MA, Report No. 3528, Apr. 1977.
5. McRuer, Duane T., and E. S. Krendel, Mathematical Models of Human Pilot Behavior, AGARDograph No. 188, Jan. 1974.
6. Zacharias, G. L., and L. R. Young, Manual Control of Yaw Motion with Combined Visual and Vestibular Cues, presented at 13th Annual Conf. on Manual Control, M.I.T., Cambridge, MA, 15-17 June 1977.
7. Magdaleno, Raymond E., and R. Wade Allen, Modeling Biodynamic Effects of Vibration, AFOSR 75-1236 TR, July 1975.
8. Ashkenas, I. L., H. R. Jex, and D. T. McRuer, Pilot-Induced Oscillations: Their Cause and Analysis, Northrop Corp., Norair Div., Rept. NOR 64-143, June 1964 (AD 481994).